*Plant Biotechnology Journal*

WILEY | aab SEB

RESEARCH ARTICLE OPEN ACCESS

# KRP3 Stability Controls Rice Plant Architecture and Productivity via MPK3-Mediated Phosphorylation

Gopal Banerjee | Sarvesh Jonwal | Balakrishnan Rengasamy | Uttam Pal | Dhanraj Singh | Mohit Mohit | Alok Krishna Sinha

BRIC-National Institute of Plant Genome Research, New Delhi, India

**Correspondence:** Alok Krishna Sinha (alok@nipgr.ac.in)

**Received:** 5 February 2025 | **Accepted:** 11 September 2025

**Funding:** The work is partially supported by the grant from the Department of Biotechnology, Government of India (Grant No.: BT/PR26207/GET/119/120/2017).

**Keywords:** cell cycle | *KRP3* | *MPK3* | proteasome | rice | seed number | tiller | orphan gene | ubiquitination

## ABSTRACT

Yield is a critical agronomic trait in cereal crops, shaped by factors like tiller and seed number, and seed weight. Understanding the factors governing these traits will help in improving the yield of plants. In this study, we identified an orphan gene, *KRP3*, belonging to cereal crops as a key regulator of rice plant architecture. Altered KRP3 protein homeostasis affected plant height, tiller number, and seed production, highlighting its role in maintaining rice plant vigor and productivity. The stability of the KRP3 protein is positively regulated by MPK3-mediated phosphorylation, as unphosphorylated KRP3 is targeted for degradation via the ubiquitin-proteasome pathway. Our findings reveal that the identified *MPK3-KRP3* module operates as an S-phase checkpoint, modulating the pace of cell division in the actively dividing zones and maintaining a balance between cell division and elongation. These findings provide valuable insights for improving plant growth and grain yield in rice.

## 1 | Introduction

Yield potential and quality are one of the most important criteria for grain crops like rice. The yield of a crop is directly regulated by four major traits, that is, tiller number, panicle number, seed number per plant, and seed size or weight (Li et al. 2021; Lo et al. 2020). To date, multiple factors are known to regulate these key traits, which include several transcription factors, phytohormones, cell division regulators, the MAP kinase signalling pathway, the ubiquitin-proteasome pathway, and so on (Burgess et al. 2023; Li et al. 2021). Out of all these factors, how the cell division machinery, MAP kinase signalling components, and the ubiquitin-proteasome pathway co-regulate rice yield traits is still an open question.

A group of plant-specific cell cycle inhibitors, known as inhibitor of cyclin-dependent kinase (ICK) or kip related protein (KRP), is known for maintaining distinct plant architecture and responses to stress (D'Ario et al. 2021). Alteration in the expression of these KRPs leads to architectural modification in rice. *KRP1* overexpression showed longer cell size in the leaf along with small seed size (Barrôco et al. 2006). Another report of the *krp2* mutant, together with the *krp1krp2* double mutant, also showed reduced grain filling, leading to a smaller grain size as well as a low germination rate (Ajadi et al. 2020). A lower seed setting rate was also observed in rice *krp4* and *krp5* mutants (Xu et al. 2023).

For keeping the cell division on the go, the protein levels of KRPs at different cell cycle stages are strictly regulated, predominantly by ubiquitination-mediated proteasomal degradation. FBL17, an F-Box-like protein, has been found to interact with multiple KRPs like KRP4, KRP6, and KRP7 and mediate their degradation (D'Ario et al. 2021; Pan et al. 2021). Other than FBL17, other E3 ligases such as $SCF^{SKP2b}$, RING protein RPK, along with UBL/UBA protein RAD23B, target KRP1 (Li

et al. 2020). In the monocot system, the mechanism maintaining KRP protein level is mostly unknown, except for a recent report of F-box protein 3 (FB3) mediated proteolysis of KRP4 and KRP5 in rice (Xu et al. 2023).

Like cell division regulatory machinery, mitogen-activated protein kinase (MAPK) signalling is also a conserved signalling cascade involved in regulating diverse pathways associated with organ development and stress responses (Jonwal et al. 2022; Manna et al. 2023; Verma et al. 2024). In rice, the *OsMKKK10-OsMKK4-OsMPK6* module regulates grain size and number as well as leaf angle by targeting WRKY53 as a BR response signal (Tian et al. 2021). This kinase module is negatively regulated by grain size and number 1 (GSN1)/MAP kinase phosphatase 1 (MKP1). It was also observed that the larger seed size in *gsn1* is due to a high cell division rate with no effect on cell elongation (Guo et al. 2018). Though MAP kinase-mediated cell cycle alteration has been observed, no direct target of cell cycle protein was known in plants until recently, where WEE1 and SMR1 are phosphorylated by MPK3 and MPK6 under UV-B exposure (Banerjee et al. 2023). Another report suggests that MPK3, MPK4, and MPK6 target E2F2, an E2F family transcription factor, and negatively regulate the activity of those transcription factors (Singh et al. 2023). These three MAP kinases also phosphorylate CDKD and govern its function in miRNA biogenesis (Singh, Verma, et al. 2024).

In this study, *KRP3* emerged as a key regulator of rice plant height, tillering, and seed number. Comparative analysis of reported KRP sequences across various monocot families indicated that *KRP3* is an orphan gene belonging to the Poaceae family. Detailed phenotypic and molecular analyses, using the generated *KRP3* mutant and overexpression lines, suggest that KRP3 protein homeostasis regulates rice architecture by regulating the rate of cell division in actively growing rice organs. Further investigation revealed that MPK3 interacts with and phosphorylates KRP3 at Ser 17 and 82 positions. Phosphorylation at these sites inhibits KRP3 ubiquitination, protecting it from proteasomal degradation. Analysis of *mpk3* mutant plants and *krp3mpk3* double mutants confirmed that *MPK3* acts upstream of *KRP3* to regulate rice plant architecture and seed number. Finally, comparative studies using overexpression lines of $KRP3^{AA}$ (phospho-dead form) and $KRP3^{EE}$ (phospho-mimetic form) show that overexpression of $KRP3^{EE}$ has a more profound effect in reducing rice organ size. Findings of the study confer that phosphorylation of the *KRP3* by *MPK3* is necessary to maintain KRP3 protein homeostasis, which in turn regulates rice architecture.

## 2 | Results

### 2.1 | KRP3 Is Involved in Regulating Rice Organ Size

In this study, we have constructed a detailed phylogenetic tree with all KRPs reported from monocot plants (Figure 1A). It was interesting to observe that *KRP1*, *KRP4*, and *KRP5* are present consistently over 22 genera, while *KRP3* and *KRP6* have been reported in 9 and 12 genera, respectively, which belong specifically to the Poaceae family. This finding suggests that *KRP3* and *KRP6* are two orphan genes restricted to the family of Poaceae. *In silico* analysis of the expression preference of both *KRP3* and *KRP6* showed that *KRP3* has a more contrasting expression pattern than *KRP6* in various tissues of rice; hence, we selected *KRP3* for further study (Figure S1A). Expression analysis of *KRP3*, using qRT-PCR analysis, in different rice tissues also suggested that *KRP3* preferentially expresses in actively growing rice tissues like seedling, emerging leaf, internode, and developing panicle (Figure S1B). To elucidate the functionality of *KRP3*, a knockout and overexpression line of *KRP3* was developed in the background of japonica rice variety TP309. *krp3* knockout mutants were developed using the CRISPR-Cas9 tool. Out of all the mutant lines identified for *KRP3*, two independent lines with either single nucleotide insertion (*krp3-1*) or deletion (*krp3-2*) in a homozygous allelic condition were selected for the study (Figure S2A–D). For *KRP3* overexpression lines, *KRP3* was expressed under the CaMV35S promoter, and three independent lines showing the highest *KRP3* expression were selected for this study (Figure S1E,F). Plants transformed with the pCAMBIA1300 vector were used as Vector Control (VC) (Figure S1G).

A comparative analysis of multiple morphological traits for the *krp3* mutant and *KRP3-OE* lines was conducted. Both *krp3-1* and *krp3-2* showed 17% and 12% reduction, respectively, in their height, compared to TP309 (Figure 1B,C). *KRP3* overexpressed plants also showed a significant (~15%) reduction in height compared to TP309 and VC plants. Plant height of TP309 and VC was comparable (Figure 1B,C). A similar pattern of reduction was observed in the case of tiller number and first internode length. Though *KRP3-OE* lines showed a minor reduction in tiller number (~10%), a significant reduction was observed in *krp3-1* and *krp3-2* lines (37% and 43%, respectively) (Figure 1D). The length of the first internode of *krp3* mutants and *KRP3-OE* lines was significantly reduced by 26% and 20%, respectively, as compared to TP309 and VC plants (Figure 1E). To determine the tissue-specific expression of *KRP3*, *ProKRP3*::*GUS* line along with VC-GUS line was developed (Figure S3A,B). A strong GUS activity was detected in immerging leaf, elongating internodes, as well as in the early panicle development stage of *ProKRP3*::*GUS* line indicating tissue-specific expression of KRP3 in the active cell division zone (Figure S3C). Internode cell length was measured for the TP309, *krp3-1*, *krp3-2*, VC, *KRP3-OE1*, *KRP3-OE2*, and *KRP3-OE3* lines to determine the effect of *KRP3* mutation and overexpression (Figure S3D). A significant increase in cell length was observed in *krp3* mutants as well as overexpression lines (Figure 1F).

After the vegetative growth parameters, yield-related traits were evaluated in all the lines. *krp3-1* and *krp3-2* lines exhibited significant reductions (10% and 12%, respectively) in maximum seed number in the primary panicle compared to TP309 and VC, while the reduction was more pronounced in *KRP3-OE* lines (35%, 21%, and 32%, respectively) (Figure 1G,H). Further, precise measurement of seed weight revealed no change in *krp3* mutant seeds compared to TP309, but *KRP3-OE1*, *KRP3-OE2*, and *KRP3-OE3* exhibited reduced seed length and weight (6%–8%) (Figure 1I, Figure S4A–C). Overall, the data indicated that tissue-specific expression of *KRP3* influences rice growth and development.

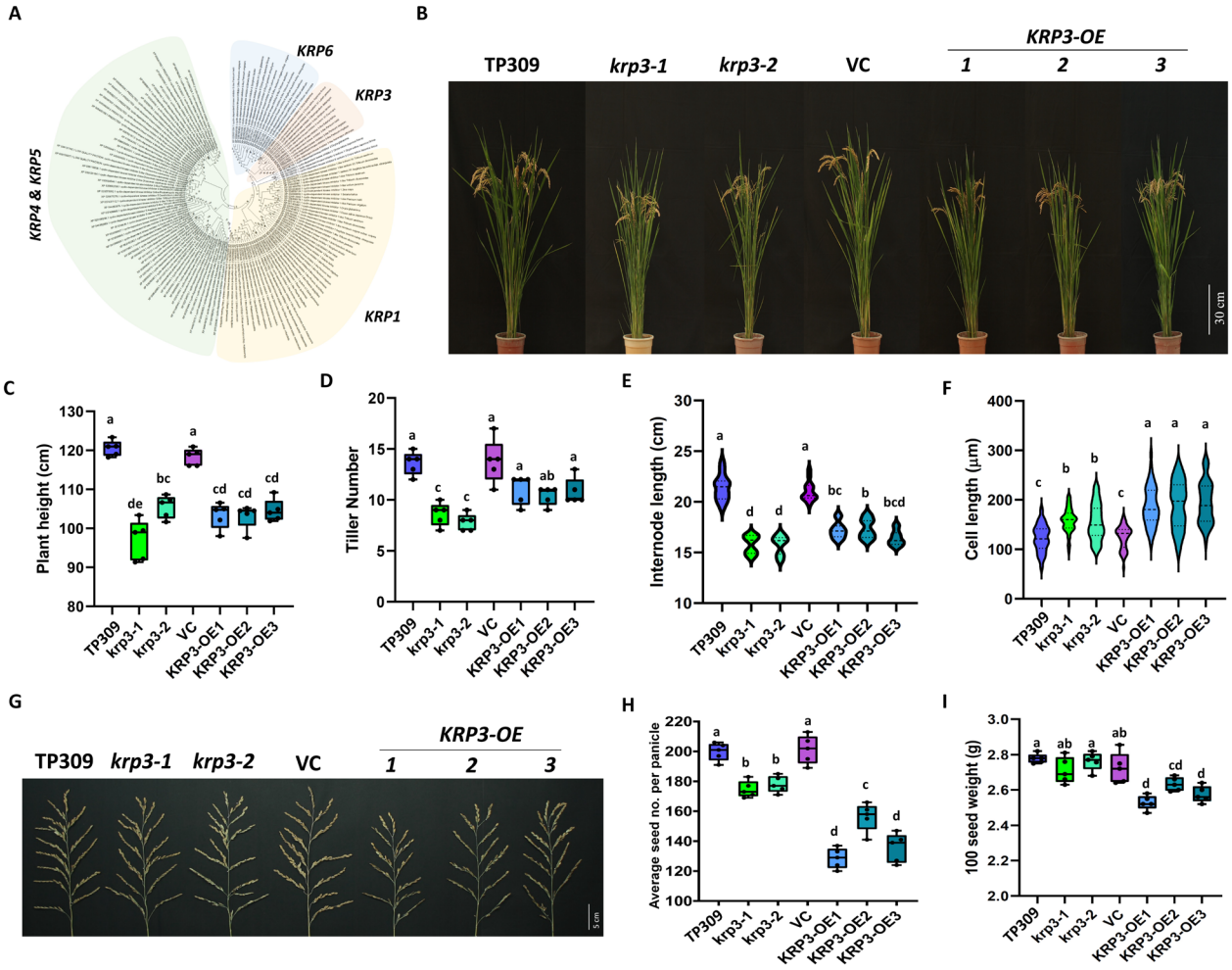


**FIGURE 1** | *KRP3* regulates rice vegetative growth and yield. (A) The phylogenetic tree developed using the protein sequence showed four major groups. KRP4 and KRP5 were found to be grouped together while other KRPs like KRP1, KRP3, and KRP6 were grouped separately. Out of all, KRP3 and KRP6 came out to be Poaceae-specific KRPs. (B) Pictorial image of TP309, *krp3-1*, *krp3-2*, VC, KRP3-OE1, KRP3-OE2, and KRP3-OE3 mature plants, respectively. (C, D) Box plot representing the plant height (C) and tiller number (D) of all the lines ($n = 5$). (E) Violin plot showing the 1st internode length of all the lines ($n > 20$). (F) Violin plot depicting the intermodal parenchyma cell length of the studied lines ($n = 50$). (G) Mature panicle of all the lines showing the difference in seed number. (H, I) Average seed number of the primary panicle (H) and 100 seed weight (I) of all the lines ($n = 5$). One-way ANOVA and Tukey's multiple comparisons test were conducted to compare the differences. Different letters represent significant changes observed in Tukey's multiple comparisons test.

## 2.2 | KRP3 Regulates Cell Proliferation in Rice Root

Fourteen-day-old seedling morphology of the *krp3* mutant as well as overexpression lines exhibited shorter shoot and root lengths compared to TP309 (Figure S4D–F). GUS activity assay demonstrated strong GUS activity in the root tip, emerging leaf, and crown region of the *ProKRP3::GUS* line, suggesting that *KRP3* plays an important role in actively dividing cells in the growing seedling (Figure S4G,H). To understand the cause of root growth retardation, cell length and width were measured from the differentiation zone of the root (Figure S5A). It was observed that the cell length of *KRP3* mutant and *KRP3-OE* lines was nearly double that of TP309 (Figure 2A). However, only *KRP3-OE* lines showed wider cells compared to TP309 and *krp3* mutants (Figure 2B). To determine the frequency of cell division, an EdU incorporation assay was conducted. A significantly lower rate of cell proliferation (33%–35%) in the root tips of the *krp3* mutant and overexpression lines was observed compared to TP309 (Figure 2C,D). A similar trend of low EdU incorporation was observed in the growing shoots of the *krp3* mutant and *KRP3-OE* compared to TP309, indicating a lower rate of cell division in the mutant and overexpression lines (Figure S5B). Results obtained from the EdU incorporation assay were further validated by determining the 2C:4C ratio in the *krp3* mutant and *KRP3-OE* lines (Figure S5A). Higher 2C levels were observed in *krp3-1*, *krp3-2*, and *KRP3-OE* lines compared to TP309 and VC, indicating a lower rate of cell division resulting from inhibition in the initiation of the S phase (Figure 2E).

To study the involvement of *KRP3* in S-phase and M-phase checkpoints, Hydroxyurea (HU), Mimosin (S-phase inhibitors), and Propyzamide, Oryzalin (M-phase inhibitors) were used. *KRP3* transcript abundance was found to be 20–25-fold higher in S-phase inhibitor-treated roots, whereas a minor change was observed in M-phase inhibitor-treated roots compared to control

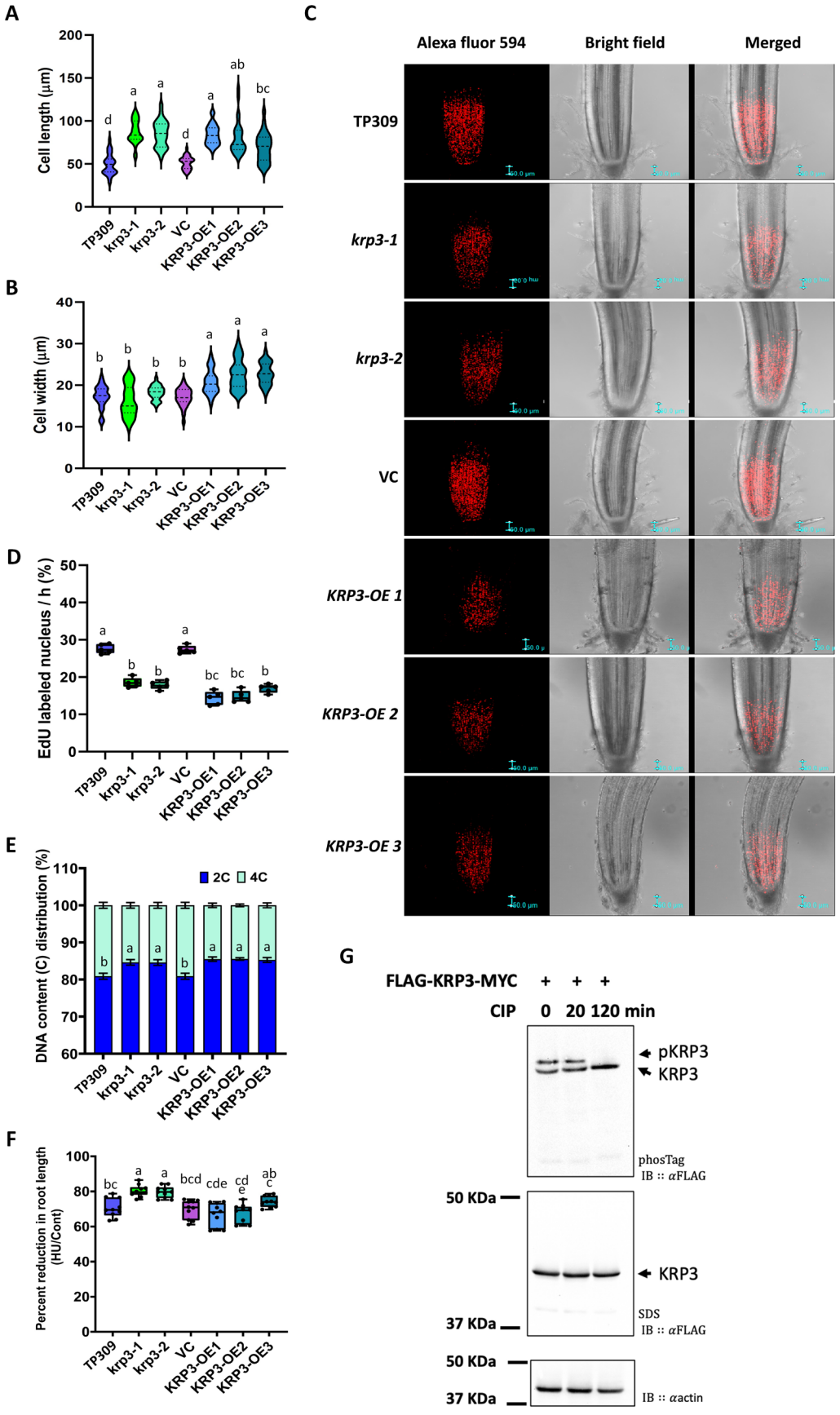


**FIGURE 2** | Legend on next page.

**FIGURE 2** | KRP3 maintains cell proliferation by regulating the G-S checkpoint. (A, B) Violin plot depicting mature root cell length (A) and width (B) of the differentiation zone of TP309, *krp3-1*, *krp3-2*, VC, *KRP3-OE1*, *KRP3-OE2*, and *KRP3-OE3* lines ($n = 30$). Though cell width was unaffected in *krp3-1* and *krp3-2*, *KRP3* knockout as well as overexpression lines showed longer cell length, indicating extended cell elongation. (C) *Z*-stacked image of Alexa Fluor 594 coupled, EdU labelled rice root as observed under a confocal microscope. The seedling was incubated for 4 h with 25 μM EdU in 1/4xMS nutrient media. (D) Box plot showing the percentage of EdU labelled nuclei, per hour, out of total nuclei, at the root division zone. (E) Bar graph representing the percentage of cells with 2C and 4C genomic content in root tips of the studied lines ($n = 5$). (F) Percent root length reduction in the presence of HU in growth media ($n = 20$). *krp3-1* and *krp3-2* showed hypersensitivity towards HU. (G) Detection of KRP3 phosphorylation using the *KRP3-OE1* line. Upshift in the KRP3 band was detected in western blot analysis using Phos-tag. No such upshift was observed in the western blot without Phos-tag, indicating phosphorylation of KRP3. No upshift of KRP3 was observed upon CIP treatment for 120 min. One-way ANOVA and Tukey's multiple comparisons test were conducted to compare the differences. Different letters represent significant changes observed in Tukey's multiple comparisons test.

(Figure S5D). Further, HU sensitivity assay was employed to evaluate the role of *KRP3* as an S-phase checkpoint regulator. *krp3-1* and *krp3-2* exhibited a strong reduction in root growth compared to TP309, indicating hypersensitivity towards HU (Figure 2F). No significant change in root length was observed in *KRP3-OE* lines when compared to TP309 and VC lines in the presence of HU (Figure 2F). HU-treated roots of *KRP3* mutants exhibited shorter cell length compared to TP309, which further explains the reduction in root length (Figure 2G). Interestingly, no significant change was observed in cell length and width of HU-treated *KRP3-OE* lines compared to TP309 and VC roots (Figure S5E,F). Considering kinases are well-known regulators of cell division, the possibility of KRP3 getting phosphorylated was evaluated using Phos-tag SDS-PAGE of the *KRP3-OE1* line. An upshift in KRP3 protein was observed in Phos-tag SDS-PAGE, unlike the control SDS-PAGE, detected using WB analysis with anti-FLAG antibody. The upshift of KRP3 was also found to be abolished upon treatment with Calf Intestine Phosphatase (CIP) (Figure 2G). The analysis of various transgenic lines demonstrated that the KRP3 protein level plays a crucial role in regulating cell proliferation during S-phase progression. Additionally, findings from the Phos-tag SDS-PAGE analysis indicate a potential post-translational regulation of the KRP3 protein.

## 2.3 | KRP3 Is a Target of MAP Kinase Mediated Phosphorylation

The MAP kinase cascade has been demonstrated to regulate rice plant height as well as seed number and size (Guo et al. 2018). This signalling cascade has also been reported to regulate cell division (Banerjee et al. 2023; Singh et al. 2023). First, the interaction of KRP3 with MAP Kinases was examined. A Y2H study of KRP3 with MPK3, MPK4, and MPK6 indicated a specific interaction of MPK3 with KRP3 (Figure 3A). The specificity of the KRP3-MPK3 interaction was further validated using an in vitro pull-down assay. For this assay, GST-tagged KRP3 was used to co-purify His-tagged MPK3, MPK4, or MPK6. Western blot of output samples showed that only MPK3 got co-purified with KRP3 (Figure 3B), validating the findings of the yeast two-hybrid assay. The identified interaction was further verified *in planta* using split luciferase complementation (SLC) and bimolecular fluorescence complementation (BiFC) assays. For the BiFC assay, KRP3 cloned with the nYFP fraction along with MPK3 and MPK6 with the cYFP fraction were co-infiltrated into *N. benthamiana* leaves. The YFP signal was observed under a confocal microscope only when KRP3 was co-infiltrated with MPK3 (Figure 3C). SUB1A1, a previously known interacting partner of MPK3, was used as a positive control (Figure 3C) (Singh and Sinha 2016). For the SLC assay, KRP3 was cloned with the C-terminal domain of firefly luciferase, while MPK3 and MPK6 were cloned with the N-terminal domain. Luminescence generated by luciferase using luciferin as a substrate was observed corresponding to the site where KRP3 was infiltrated with MPK3. The SUB1A1-MPK3 combination was used as a positive control while the KRP3-MPK6 combination was used as a negative control (Figure 3D). The stringency of this interaction was further evaluated using a co-immunoprecipitation assay where KRP3 tagged with N-ter 3xFLAG and C-ter 4xMYC were co-infiltrated with GFP, GFP-tagged MPK3, and MPK6. Western blot analysis with the immunoprecipitated proteins demonstrated that only MPK3 co-immunoprecipitated with KRP3 confirming the *in planta* interaction of MPK3 and KRP3 (Figure 3E).

To determine the KRP3 phosphorylation by MPK3 and to find out the exact site of phosphorylation, an in vitro kinase assay was employed. KRP3 was used as the substrate, while MPK3, or AtMKK4$^{DD}$-activated MPK3, was used as an upstream kinase. Trans-phosphorylation activity of MPK3 and AtMKK4$^{DD}$-activated MPK3 was confirmed using Myelin basic protein (MBP) as a substrate and GST as a negative control. In vitro kinase assay results depict that MPK3 was able to phosphorylate KRP3 (Figure S6A). After confirmation of KRP3 as a phosphorylation target of MPK3, the exact site of phosphorylation was investigated. Four possible phosphorylation sites, S17, S82, S112, and S168 identified in silico, were taken for consideration (Figure S6B). Four individual constructs were developed where Ser was mutated to Ala in three identified positions. An additional construct where all four Ser residues were converted to Ala was developed (Figure 3F). Phosphor image confirmed that Ser at positions 17 and 82 is the target site for MPK3-mediated KRP3 phosphorylation (Figure 3G, Figure S6C). These experiments validated that MPK3 physically interacts and phosphorylates KRP3.

## 2.4 | KRP3 and MPK3 Function in a Linear Pathway

Once it was established that KRP3 is a phosphorylation target of MPK3, the dynamics of this interaction were checked *in planta* using *mpk3* as well as *krp3mpk3* double mutant plants. Mutants for *MPK3* were developed using CRISPR-Cas9, and

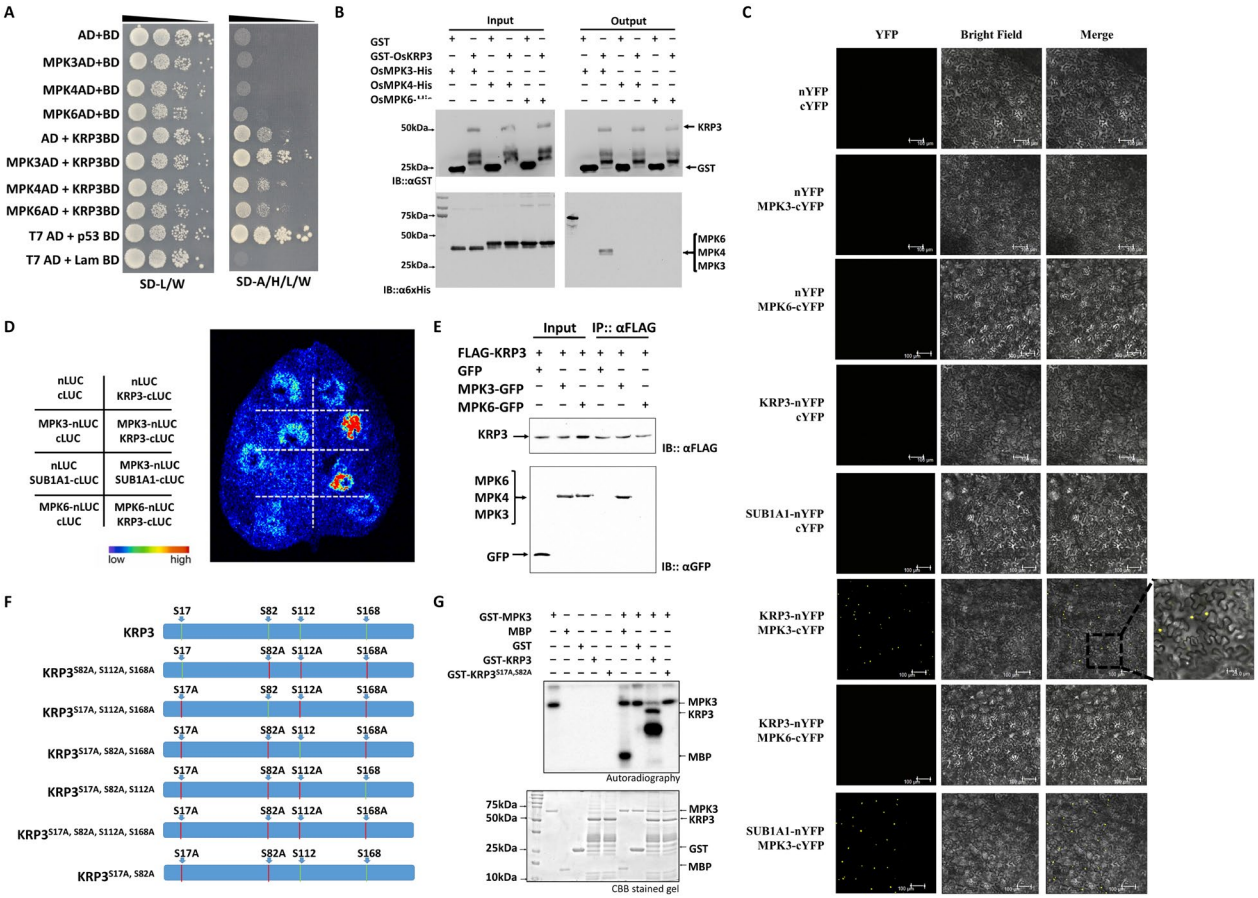


**FIGURE 3** | MPK3 interacts and phosphorylates KRP3 at S17 and S82 positions. (A) Yeast two-hybrid interaction assay of KRP3 with MPK3, MPK4, and MPK6. KRP3 was cloned with GAL4 DNA binding domain (BD), while MAP kinases were cloned with the activation domain (AD). (B) In vitro pull-down assay using GST-KRP3 as prey and MAP kinase as a bait shows that MPK3 gets co-purified by GST-KRP3, unlike the other two MAP kinases. (C, D) Split luciferase complementation (SLC) assay and bimolecular fluorescence complementation (BiFC) assay demonstrating *in-planta* interaction of KRP3 and MPK3. For the SLC assay, *KRP3* and *SIB1A1* were cloned into pCAMBIA-cLUC vectors while *MPK3* and *MPK6* cloned into the pCAMBIA-nLUC vector. *KRP3* and *SIB1A1* were cloned in pSPYNE(R)173 vectors, while *MPK3* and *MPK6* cloned into pSPYCE(M) were used for the BiFC assay. SUB1A1-MPK3 combination was used as a positive control, while the KRP3-MPK6 combination was used as a negative control in both experiments. (E) Co-IP assay of GFP, GFP-MPK3, and GFP-MPK6 by KRP3, using anti-FLAG antibody. WB results confirm that only GFP-MPK3 gets co-precipitated with KRP3, and not GFP or GFP-MPK6, confirming the interaction of KRP3 and MPK3. (F) Diagrammatic representation of KRP3 protein structure and position of SP motifs within the protein along with different site-directed mutagenesis constructs developed to confirm the phosphorylation site of KRP3. (G) In vitro kinase assay of MPK3 using KRP3 as substrate. MBP was used as a positive control and GST as a negative control for the kinase assay. The kinase assay was repeated three times, and similar results were observed.

two independent lines with single-nucleotide addition or deletion were selected for further study (Figure S7A–D). Both *mpk3-1* and *mpk3-2* exhibited an indifferent trend of reduced plant height, tiller number, seed number, and seed weight (Figure S8A–F). Further, *krp3mpk3* double mutant was generated, and a single line with a single nucleotide addition similar to that of *krp3-1* and *mpk3-1* was selected (Figure S9A,B). Reduction in plant height was evident in *mpk3-1* and *krp3mpk3* double mutant. Where *mpk3-1* exhibited a 6% reduction in plant height, *krp3-1* and *krp3mpk3* showed a 15% reduction to that of TP309 (Figure 4A,B). Evaluating *krp3mpk3* for internode length and tiller number with TP309, internode length was found to be shorter by 19% and tiller number was lowered by 38%, a trend similar to *krp3-1* (Figure 4C,D). Careful evaluation of the internode cell length of TP309, *krp3-1*, *mpk3-1*, and *krp3mpk3* indicates that *krp3-1* and *krp3mpk3* have significantly longer cell length compared to TP309 (Figure 4E). The reduction in seed number was more pronounced in *krp3mpk3* (11%) compared to TP309, like *krp3-1*, while the reduction in seed number in *mpk3-1* was nearly 8% (Figure 4F,G). Unlike seed number, no change in seed size or weight was evident in the mutant lines compared to control plants (Figure S9C–F). Overall, the observations suggested that *MPK3* works upstream of *KRP3* in regulating plant growth and development.

## 2.5 | MPK3 Assists KRP3 in Maintaining Cell Division Rate

To elucidate the effect of *mpk3* and *krp3mpk3* on the growth of rice seedlings, shoot and root lengths of 14-day-old seedlings were evaluated. The *krp3mpk3* mutants showed a significant reduction in both shoot (14%) and root length (29%) compared to TP309, while *mpk3-1* exhibited minimal effect on shoot and root length reduction (Figure S10A–C). Additionally, no statistically significant differences were observed between shoot

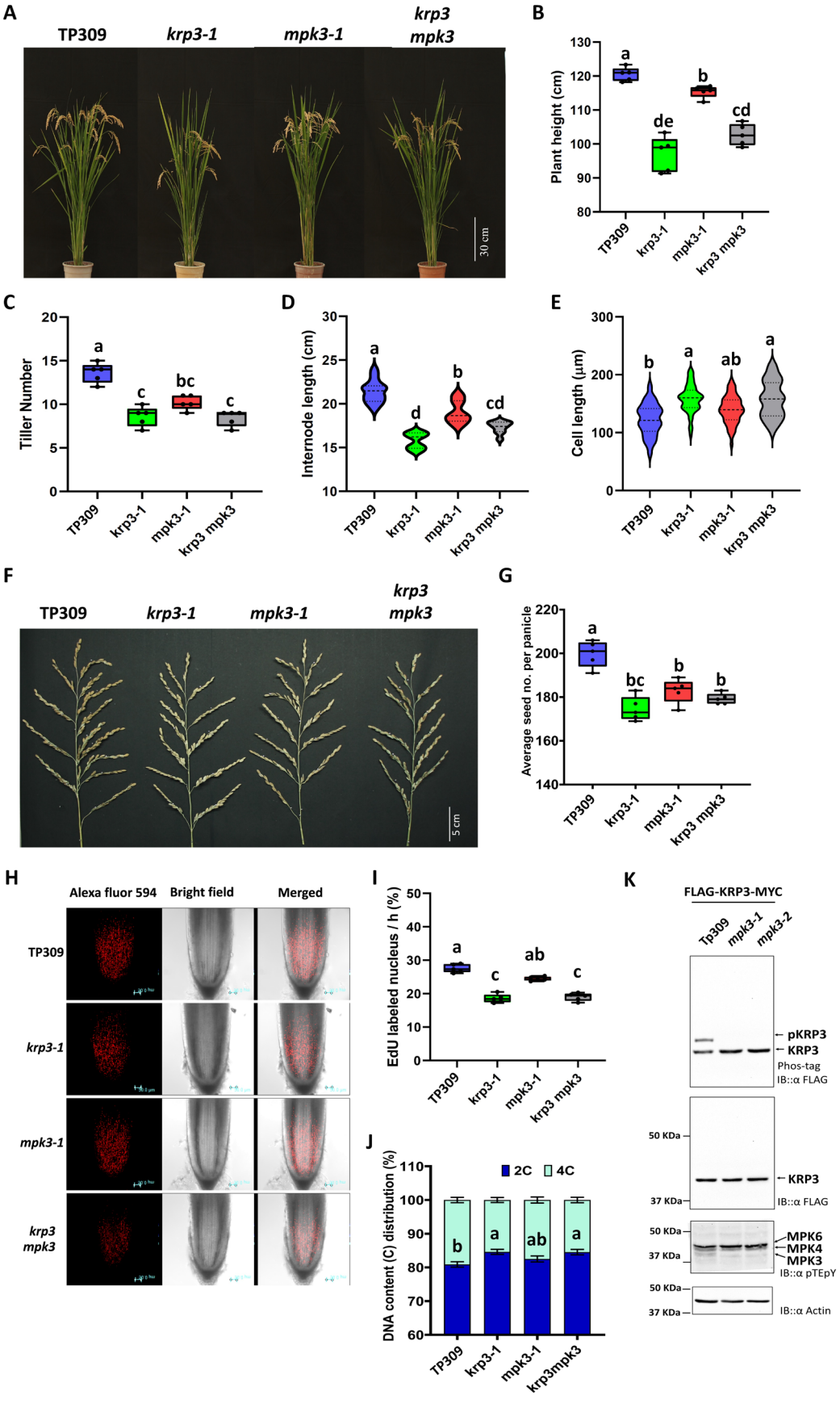


**FIGURE 4** | Legend on next page.

**FIGURE 4** | *KRP3* and *MPK3* work in compliance. (A) Pictorial representation of TP309, *krp3-1*, *mpk3-1*, and *krp3mpk3* mature plants, respectively. (B, C) Box plot representing the plant height (B) and tiller number per plant (C) ($n = 5$) of the respective lines. (D, E) Violin plot representing 1st internode length (D) ($n > 20$) and internode cell (parenchyma) length (E) ($n = 50$) of the studied lines. (F) Representative image of a mature panicle of the respective lines. (G) Box plot depicting the average seed number of the primary tiller of all the studied lines ($n = 5$). (H) *Z*-stacked image of the Alexa fluor 594 coupled, EdU labelled root tip of TP309, *krp3-1*, *mpk3-1*, and *krp3mpk3* as observed under a confocal microscope. Roots were incubated with 25 μM EdU in 1/2xMS media for 4 h. (I) Quantitative box plot showing the percentage of EdU labelled nuclei out of all visible nuclei at the root division zone of the respective lines. (J) Bar graph representing the genomic content distribution ratio (2C:4C) in the root tips of the studied lines ($n = 5$). (K) Detection of the KRP3 phosphorylation profile in TP309, *mpk3-1*, and *mpk3-2* backgrounds. IB analysis of KRP3 protein, using anti-FLAG antibody, resolved using 40 μM Phos-tag in 8% SDS polyacrylamide gel, shows an up-shift in KRP3 protein only in the TP309 background. A single band of KRP3 was confirmed in the counter SDS polyacrylamide gel without Phos-tag. IB with anti-pTEpY antibody confirms no activity of MPK3 in the *mpk3* mutant background. IB with anti-Actin indicates equal protein concentration in all the wells. The experiment has been repeated three times and similar results were found. One-way ANOVA and Tukey's multiple comparisons test were conducted to compare the differences. Different letters represent significant changes observed in Tukey's multiple comparisons test.

and root length of *krp3-1* and *krp3mpk3* (Figure S10B,C). The root cell length in *krp3-1* and *krp3mpk3* was found to be similar, that is, 1.6-fold longer cell length than that of TP309 (Figure S10D). The *mpk3-1* also exhibited moderately longer cell length (1.2-fold), with respect to TP309 (Figure S10D). Expression of all KRPs was also studied in the mutant background at seven-day-old seedling stage and compared to that of TP309 (Figure S10E). Higher expression of all 6 KRPs was evident in the *mpk3-1* background. In the *krp3-1* background, a near three-fold expression of KRP1 and two-fold expression of *KRP4* was observed, but no such trend was observed in the *krp3 mpk3* mutant line (Figure S10E) This data suggests that other KRPs are not responsible for the reduced growth rate of *krp3* mutant and OE lines.

The rate of cell division in *krp3-1*, *mpk3-1*, and *krp3mpk3* root and shoot tips was assessed using EdU labeling and compared to TP309. *krp3-1* and *krp3mpk3* exhibited a drastic (30%) reduction in EdU-labelled cells relative to TP309, while *mpk3-1* exhibited a moderate reduction in nuclei labeling (Figure 4H,I, Figure S10F). This trend of reduced cell division was also reflected in the increased 2C:4C ratio in the root tips of *krp3-1* and *krp3mpk3* compared to TP309, as determined by flow cytometry analysis (Figure 4J, Figure S10G). Finally, to confirm that KRP3 is phosphorylated by MPK3 as a downstream substrate, the phosphorylation profile of the KRP3 protein was analyzed in the TP309, *mpk3-1*, and *mpk3-2* backgrounds using Phos-tag PAGE. Like before, a clear upshift of phosphorylated KRP3 protein was detected in the *KRP3-OE1* background, while no such upshift was detected when FLAG-KRP3 was transiently expressed in the *mpk3-1* and *mpk3-2* backgrounds (Figure 4K). Additionally, western blot analysis using the anti-pTEpY antibody confirmed the absence of MPK3 protein in the *mpk3-1* and *mpk3-2* backgrounds (Figure 4K). These observations validate our previous observation that KRP3 is indeed a phosphorylation target of MPK3.

## 2.6 | Phosphorylation of KRP3 Leads to More Sturdy Cell Cycle Inhibition

To assess the impact of KRP3 phosphorylation on plant growth and yield, transgenic rice lines overexpressing phospho-dead ($KRP3^{S17A,S82A}$) and phospho-mimetic ($KRP3^{S17E,S82E}$) variants of *KRP3* were generated. Three independent lines of each variant, showing comparable KRP3 overexpression with KRP3-OE lines, were selected for further analysis and named $KRP3^{AA}$-*OE1/2/3* and $KRP3^{EE}$-*OE1/2/3* respectively (Figure S11A,B). Comparatively, the selected lines of $KRP3^{AA}$-*OE* and $KRP3^{EE}$-*OE* were showing a similar pattern of plant height, internode length, tiller number, and average seed number per panicle compared to TP309 (Figure S11C–L).

Among *KRP3-OE1*, $KRP3^{AA}$-*OE1*, and $KRP3^{EE}$-*OE1*, $KRP3^{EE}$-*OE1* exhibited the highest reduction in plant height (21%) and internode length (25%), while $KRP3^{AA}$-*OE1* showed the least reduction (13% and 12%, respectively). *KRP3-OE1* exhibited intermediate effects on both traits (15% and 20%, respectively) (Figure 5A–C). Among the overexpression lines, $KRP3^{EE}$-*OE1* has a significant positive effect on tiller number, while *KRP3-OE1* and $KRP3^{AA}$-*OE1* did not affect tiller number (Figure 5D). In contrast, all $KRP3^{EE}$-*OE* lines showed a significant reduction in seed number per panicle, with $KRP3^{EE}$-*OE1* showing the largest decrease (41%) (Figure 5E, Figure S11K,L). $KRP3^{AA}$-*OE1* showed the least reduction in seed number (19%) (Figure 5F). $KRP3^{AA}$-*OE* and $KRP3^{EE}$-*OE* lines both exhibited lower seed weight and length (Figure S11M–P). Comparatively, $KRP3^{EE}$-*OE1* showed the greatest reduction in seed weight (21%) and length (11%), followed by *KRP3-OE1* (8% and 7%) and $KRP3^{AA}$-*OE* (4% and 5%), which had more moderate reductions (Figure 5G – I).

On comparing seedling root cell lengths, $KRP3^{EE}$-*OE1* had the longest and widest root cells, while $KRP3^{AA}$-*OE1* had no significant difference in root cell elongation compared to TP309 and VC (Figure 6A,B). The 2C:4C DNA content ratio in root tip revealed the highest difference in$KRP3^{EE}$-*OE1*, indicating strong inhibition of S phase initiation, while *KRP3-OE1* and $KRP3^{AA}$-*OE1* showed progressively lower inhibition, with $KRP3^{AA}$-*OE1* showing the least (Figure 6C, Figure S12A). A similar trend was observed when cell division rates were measured using the EdU incorporation assay. $KRP3^{EE}$-*OE1* exhibited the strongest inhibition in cell division (66%), followed by *KRP3-OE1* (48%), while $KRP3^{AA}$-*OE1* had a minor effect (24%) (Figure 6D,E, Figure S12B). Expression of other KRPs was studied in seven-day-old seedlings of these overexpression lines and compared with TP309 and VC. *KRP1*, *4*, and *6* showed higher expressions in the *KRP3-OE1* line (Figure S12C). Higher expression of *KRP1* was also observed in the $KRP3^{AA}$-*OE1* line, and *KRP6* in the $KRP3^{EE}$-*OE1* line.

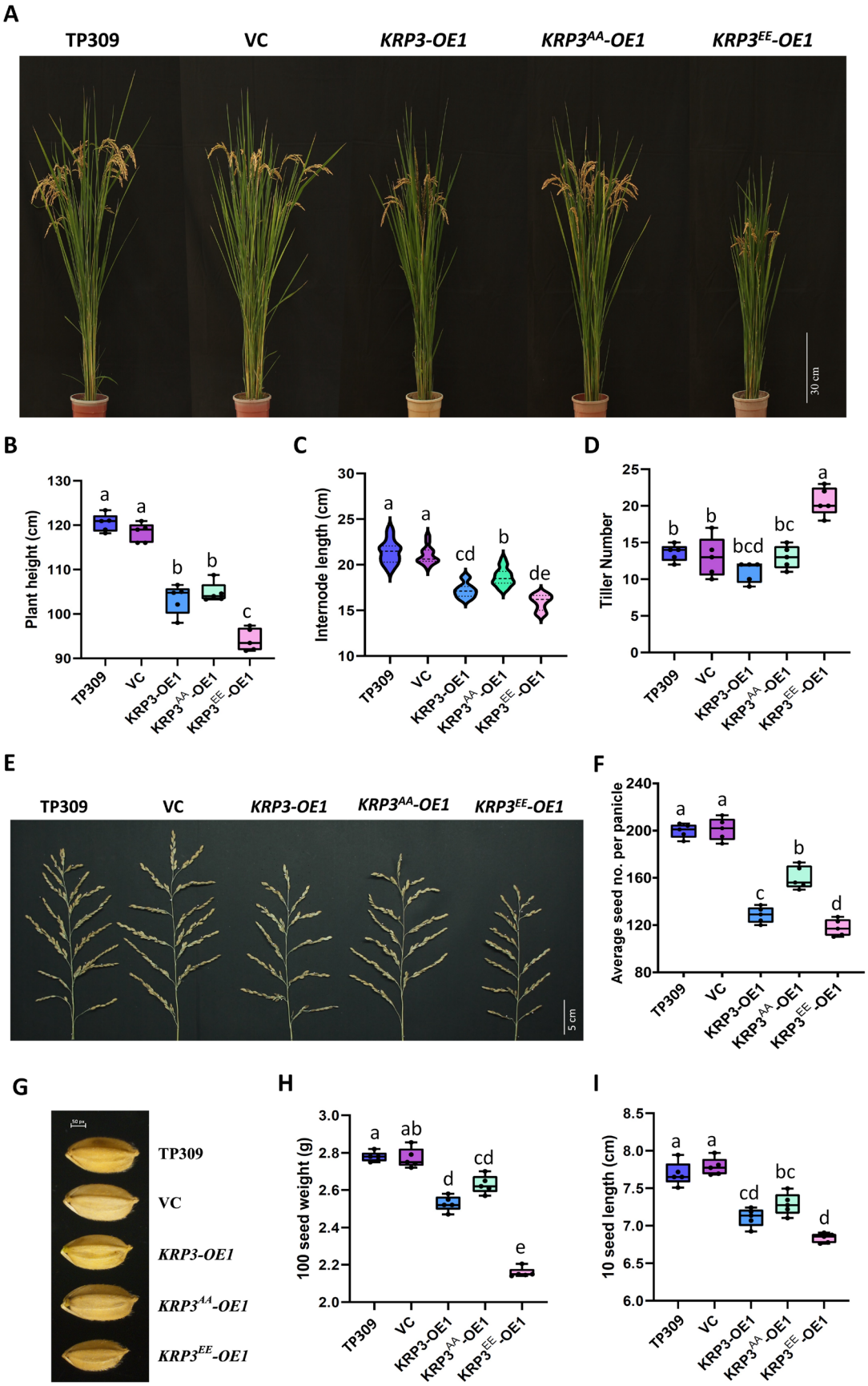


**FIGURE 5** | Legend on next page.

**FIGURE 5** | Overexpression of KRP3$^{EE}$ promotes stronger plant growth inhibition. (A) Pictorial representation of TP309, VC, KRP3-OE1, KRP3$^{AA}$-OE1, and KRP3$^{EE}$-OE1 mature plants. (B, C) Box and violin plot representing the plant height (B) ($n = 5$) and 1st internode length (C) ($n = 20$) of mature plants of all the lines. (D) Tiller number of all the lines ($n = 5$). (E) Comparative photograph of a mature panicle. (F) Average seed number of the primary tiller of the respective lines ($n = 5$). (G) Pictorial representation of seed size of TP309, VC, KRP3-OE1, KRP3$^{AA}$-OE1, and KRP3$^{EE}$-OE1. (H, I) Box plot showing seed weight (H) and seed length (I) ($n = 5$). One-way ANOVA and Tukey's multiple comparisons test were conducted to compare the differences. Different letters represent significant changes observed in Tukey's multiple comparisons test.

Though some KRPs showed elevated expression, no consistent trend was observed in their expression compared to all the overexpression lines (Figure S12C).

Finally, the phosphorylation profile of the KRP3 protein was analysed using Phos-tag SDS PAGE. An upshift in KRP3 protein was detected in the *KRP3-OE1* background but not in *KRP3$^{AA}$-OE1or KRP3$^{EE}$-OE1* (Figure 6F). Together, these data suggest that MPK3-mediated phosphorylation of KRP3 leads to substantial inhibition of the cell cycle.

### 2.7 | Phosphorylation of KRP3 Inhibits Its Proteasome-Mediated Degradation

To investigate how phosphorylation affects KRP3 function, the localization of KRP3, KRP3$^{AA}$, and KRP3$^{EE}$ was checked in *N. benthamiana* leaves. The N-terminal of KRP3 and its mutant forms were tagged with mCherry, while NLS-tagged mGFP served as a nuclear marker. Unlike mCherry alone, which was found in both the nucleus and cytosol, KRP3 and its mutant forms localized specifically to the nucleus (Figure S13A). Additionally, the effect of phosphorylation on KRP3's interaction with CDKA, CycD, and MPK3 was examined using the BiFC assay. KRP3, KRP3$^{AA}$, and KRP3$^{EE}$ were fused with the C-terminal domain of YFP and were co-infiltrated with CDKA, CycD, and MPK3 fused with the N-terminal of YFP. No change in interaction between KRP3, KRP3$^{AA}$, and KRP3$^{EE}$ with CDKA, CycD, and MPK3 was observed (Figure S13B).

The effect of phosphorylation on KRP3 protein stability was also assessed using a cell-free degradation assay. MBP-KRP3-6xHis, MBP-KRP3$^{AA}$-6xHis, and MBP-KRP3$^{EE}$-6xHis chimeric proteins were incubated with crude plant protein extract of TP309 seedling for 120 min. Western blot analysis using anti-His antibody showed that KRP3 and KRP3$^{AA}$ protein levels were decreased significantly, while the reduction in KRP3$^{EE}$ protein was less pronounced (Figure 7A, Figure S14A–C). To determine whether this degradation is proteasome-mediated, KRP3 protein stability was examined in the presence and absence of the proteasome inhibitor MG132 in a time-dependent manner. KRP3 and KRP3$^{AA}$ showed increased stability with MG132 (Figure 7B, Figure S14D,E), while KRP3$^{EE}$ protein stability was marginally affected (Figure 7B, Figure S14F). In the *mpk3* mutant background, the stability of KRP3 was reduced and was comparable to KRP3$^{AA}$ stability level in the absence of MG132 (Figure 7B, Figure S14G). An in vitro ubiquitination assay using anti-Ubi antibody confirmed that KRP3 and KRP3$^{AA}$ were poly-ubiquitinated, whereas KRP3$^{EE}$ exhibited distinguishably lower ubiquitination (Figure 7C). These observations indicate that the stronger inhibition of the cell cycle in the transgenic line overexpressing the phospho-mimetic version of KRP3 is due to phosphorylation and subsequent stabilisation of KRP3 by MPK3, which reduces its turnover.

## 3 | Discussion

In the present study, we have demonstrated the role of the *KRP3-MPK3* module in maintaining rice plant architecture and yield. Recent studies have also demonstrated the important role of cell division cycle components in regulating rice yield. Ectopic overexpression of rice *KRP1* has shown increased cell size and reduced cell division, leading to smaller leaves and ill-developed seeds with altered size and ploidy levels in the embryo (Ajadi et al. 2020; Ren et al. 2008). Other than *KRP1*, *OsiICK6* or *KRP4* overexpression in the *indica* rice variety strongly reduces organ size and grain production (Xu et al. 2023; Yang et al. 2011). Mutation of KRPs in rice, like *krp1* or *krp5*, has shown a significant effect on seed filling rate (Ajadi et al. 2020; Xu et al. 2023). To investigate the probable involvement of other cell cycle inhibitors in maintaining rice vigour and yield, we first checked the conservation of different KRPs throughout monocot families. Phylogenetic analysis of *KRP*s from monocot genera yielded some critical observations. Interestingly, *KRP3* and *KRP6* turned out to be orphan genes existing only in the Poaceae family of monocots (Arendsee et al. 2014). Orphan genes (OGs) are genes whose presence is restricted to a particular family or genus. Orphan genes are fast evolving and play a crucial role in providing developmental and environmental adaptations. With the increase in the number of sequenced plant genomes, it is evident that every plant possesses 1%–5% of OG in its genome (Arendsee et al. 2014). As OGs are fast evolving, predicting their function becomes challenging, and hence it becomes very important to functionally characterise these genes (Jiang et al. 2022). Identification of an orphan gene in an economically important crop family also indicates its importance in maintaining agronomic traits for which it has been retained during domestication (Jiang et al. 2022). Looking at the economic importance of rice, the probable role of *KRP3* in maintaining rice morphogenesis and productivity was studied. Phenotypic analysis of two independent *krp3* knock-out mutants showed reduced plant height and less tiller formation. Meticulous measurement of internode length revealed that the reduction in plant height is a consequence of shorter internodes. Reduction in plant height and tiller number in crop species is considered one of the superior traits in modern agriculture, where overall seed production per tiller is increased (Liu et al. 2018; Takai 2023). The contrasting trend of cell length in the internode region to that of internode length clearly indicated that the shortening of the internode is not due to a reduction in cell length. Rather, this trend of longer cell length in *krp3* mutants provides a hint towards an altered cell division rate (Song et al. 2022).

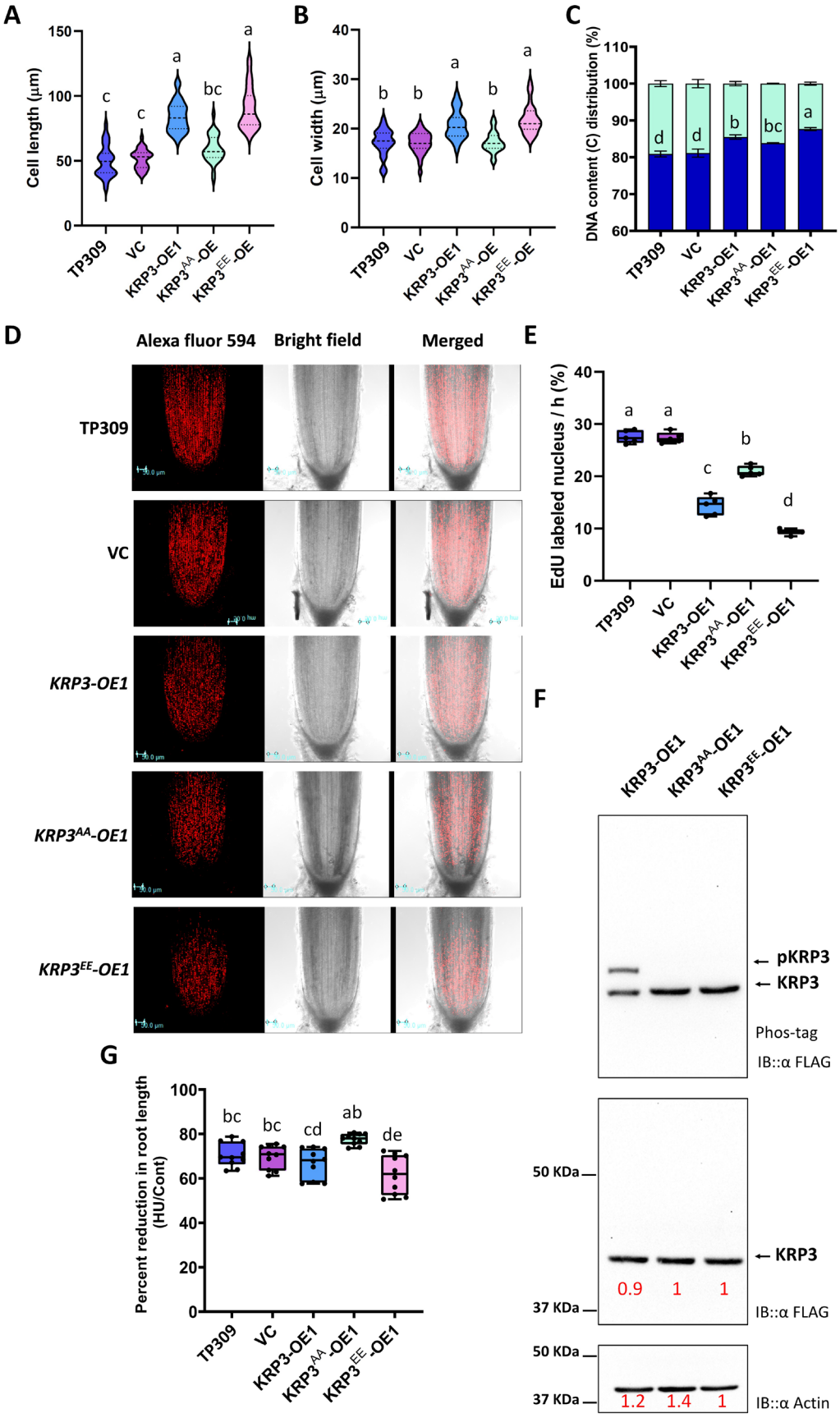


**FIGURE 6** | Legend on next page.

**FIGURE 6** | KRP3 maintains cell division rate by regulating G-S checkpoint. (A, B) Violin plot showing the root cell length (A) and width (B) at the differentiated zone of the overexpression lines compared to TP309 and VC ($n = 50$). (C) Bar graph reflecting the ratio of nucleus with 2C and 4C genomic content in TP309, VC, *KRP3-OE1*, *KRP3$^{AA}$-OE1*, and *KRP3$^{EE}$-OE1* line ($n = 5$). (D) *Z*-stacked image of Alexa fluor 594 coupled, EdU labelled root tip of TP309, VC, *KRP3-OE1*, *KRP3$^{AA}$-OE1*, and *KRP3$^{EE}$-OE1* as observed under confocal microscope. Seedling was incubated for 8 h with 25 μM EdU in 1/4xMS nutrient media. (E) Percentage of EdU labelled nucleus in 1 , out of total visible nucleus in root tips was calculated. (F) Confirmation of S17 and S82 as MPK3 mediated KRP3 phosphorylation site. Protein mobility of KRP3, KRP3$^{AA}$, and KRP3$^{EE}$ forms was detected using 40 μM Phostag SDS polyacrylamide gel (8%) and WB with anti-FLAG antibody. A single band of KRP3 was confirmed in counter SDS polyacrylamide gel without Phostag. IB with anti-Actin indicates protein concentration in all the wells. Experiment has been repeated three times and similar results were found. (G) Detection of HU sensitivity in the seedlings of all the lines. One-way ANOVA and Tukey's multiple comparisons test were conducted to compare the differences. Different letters represent significant changes observed in Tukey's multiple comparisons test.

KRP3 was also observed to play an important role in maintaining crop yield. The *krp3* mutation negatively affected the seed number per panicle. Interestingly, in *krp3-1* and *krp3-2*, though seed number was reduced, seed size and weight were unaffected. Traits such as effective tiller number, seed number, seed size, and weight are some of the key components determining rice yield (Li et al. 2021). Thus, with a reduced tiller and seed number, *krp3* plants exhibited a significant reduction in rice productivity. These observations hint towards the role of KRP3 in the regulation of crop architecture and yield.

*KRP3* overexpression lines also showed an overlapping phenotype with that of *krp3* mutants. All three studied overexpression lines of *KRP3* showed a negative effect on plant height, leaf length, tiller number, seed number, and seed weight. Displaying a similar effect in both overexpression as well as in a mutant of any gene is not unlikely and has been observed in plenty of cases where a gene executes its function in a dose-dependent manner (Chen et al. 2023; Spadafora et al. 2012). KRP3 acts as a negative regulator of the cell division cycle, which justifies the reduction in overall plant size and productivity in *KRP3* overexpression lines. Similar growth compromise has been observed in both *Arabidopsis* and rice in the case of overexpression of KRP genes (Barrôco et al. 2006). However, the cause of the growth and yield penalty in *krp3* plants was not clear.

While KRP3 influences rice architecture, it was important to understand whether it was through modulating cell division rate or mature cell size. EdU is an analogue of thymidine, and it can be utilised to detect cell proliferation rates by externally supplying it in the growth media (Chehrehasa et al. 2009). The estimated cell division rate by EdU incorporation assay and the ratio of 2C:4C genomic content in the growing root tips of *krp3-1* and *krp3-2* revealed that mutation of *krp3* negatively affects cell cycle progression. This reduction in cell division led to cell elongation in *krp3-1* and *krp3-2* compared to TP309. This observation is consistent with earlier studies reporting that the inhibition of cell division leads to extended cell elongation (Song et al. 2022). *krp3* mutants also exhibited reduced root length, hinting that the elongation of root cells is not sufficient to surpass the effect of lower cell division in the dividing zone. Interestingly, the rate of cell cycle inhibition and cell elongation in *krp3* is similar to that of *KRP3* overexpression lines.

Quantitative analysis of *KRP3* transcript abundance using the cell cycle inhibitors showed that KRP3 functions specifically in S-phase checkpoint regulation. Hydroxyurea (HU) and Mimosine, two well-known inhibitors of ribonucleotide reductase, were used as S-phase inhibitors (Pan et al. 2021). For M phase inhibition, Propyzamide and Oryzalin, two anti-mitotic drugs inhibiting microtubule polymerisation, were used (Nakamura et al. 2004). The fact that KRP3 is involved in S-phase checkpoint regulation was also evident through hypersensitivity towards HU. Similar inhibition in root growth in the presence of HU has also been reported in mutants of other S-phase checkpoint regulators like *atm*, *atr*, and *wee1* (Pedroza-Garcia et al. 2021; De Schutter et al. 2007). Though *krp3* mutants were hypersensitive to HU, root length reduction in *KRP3* overexpression lines was identical to TP309, indicating a rate limitation in KRP3 function, possibly pointing towards a post-translational modification.

Post-translational modification like phosphorylation has been known for a long time to maintain the functionality of proteins (Verma et al. 2020). Recent studies have demonstrated that three MAP Kinases, MPK3, MPK4, and MPK6, phosphorylate the E2F2 transcription factor and inhibit its function in the presence of HU (Singh et al. 2023). Out of these three MPK Kinases, MPK3 specifically interacted with KRP3 in the nucleus in our study. The interaction of proteins with MPK3 often leads to its phosphorylation (Bhagat, Sharma, et al. 2022). We observed that MPK3 activated by AtMKK4$^{DD}$ can phosphorylate KRP3 and Myelin basic protein (MBP). It was also observed that bacterially expressed MPK3 showed auto and trans-phosphorylation, as MPK3, without activation by upstream MAPKK, can phosphorylate MBP as well as KRP3. Auto-activation properties of bacterially expressed MAP Kinases have been reported previously (Sethi et al. 2014; Singh and Sinha 2016). Previous reports also suggest that MAP Kinase phosphorylates its substrate at the S/TP motif (Dóczi and Bögre 2018). Four SP sites were identified as possible MAP Kinase phosphorylation sites in the KRP3 protein sequence. These putative phosphorylation sites were validated by using five combinations of KRP3$^{S>A}$ constructs as Ala is considered a non-phosphorylatable amino acid (Dóczi and Bögre 2018). In vitro kinase assay using these mutant forms suggested that MPK3 phosphorylates KRP3 at Ser 17 and S82 positions. This was further validated using a KRP3$^{S17A,S82A}$ (KRP3$^{AA}$) mutant and this mutated form of KRP3 remains unphosphorylated by MPK3.

The present study also evaluated the role of MPK3 in rice morphogenesis and yield using *mpk3* knock-out mutants. Both *mpk3-1* and *mpk3-2* exhibited phenotypes similar to the *krp3* mutant phenotype, with reduced plant height, shorter

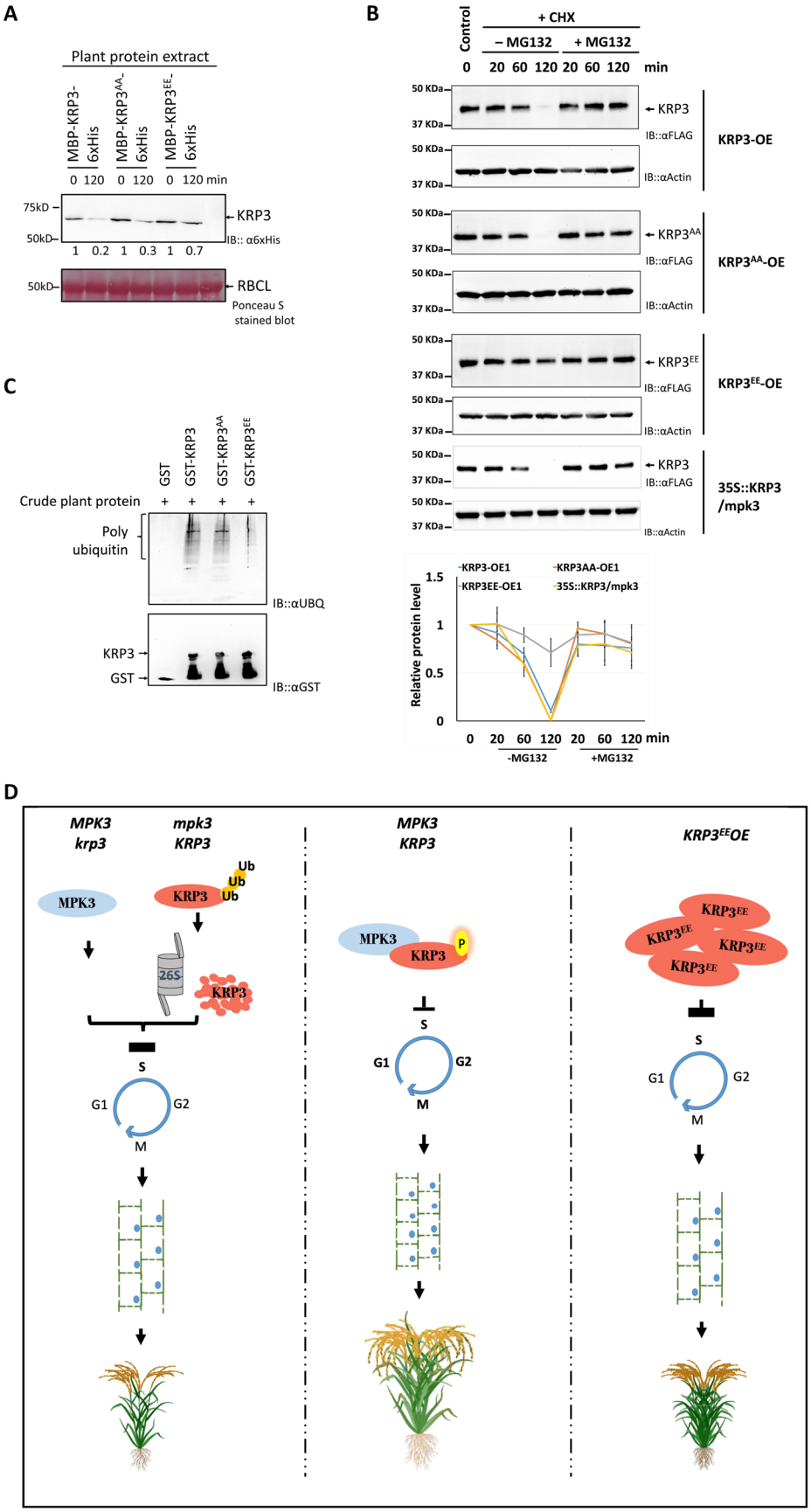


**FIGURE 7** | Legend on next page.

**FIGURE 7** | Phosphorylation of KRP3 at S17 and S82 positions promotes its stability. (A) Cell-free degradation assay of KRP3, KRP3$^{AA}$, and KRP3$^{EE}$, incubated with plant protein extract for 120 min. Western blot showing KRP3 protein level of initial and post 120 min of incubation. (B) In vivo degradation assay of KRP3, KRP3$^{AA}$, and KRP3$^{EE}$ in the presence or absence of MG132 in a time-dependent manner. Line graph indicates the relative protein level of KRP3, KRP3$^{AA}$, and KRP3$^{EE}$ compared to respective Actin level. (C) In vitro ubiquitination assay of KRP3, KRP3$^{AA}$, and KRP3$^{EE}$. (D) Model depicting how KRP3 protein homeostasis and its phosphorylation status regulate rice vigour and yield. Absence or abundance of KRP3 protein level negatively affects rice growth. It's only the adequate KRP3 protein level that is essential to maintain proper vigour and yield in rice. All three assays have been repeated over three times, and similar observations were made.

internode length, and a smaller number of tillers and seeds in the primary panicle. Though the root growth of *mpk3* mutants showed no difference in normal conditions, it showed less sensitivity to HU-mediated cell division inhibition. In the absence of MPK3, the checkpoint regulation at the G1-S phase might be hampered as it is also involved in the regulation of other checkpoint regulators (Banerjee et al. 2023). The *krp3mpk3* double mutant also exhibited a similar trend in vegetative growth parameters like reduction in plant height, internode length, and tiller number. Interestingly, there was no significant difference between *krp3-1* and *krp3mpk3* mutant lines. Similar trends were observed in the case of seed number reduction and shoot and root length reduction in 14-day seedlings. *krp3mpk3* also showed hyper HU sensitivity and reduced cell division rate like *krp3-1*. This similar trend of mutant phenotypes of *krp3-1*, *mpk3-1*, and *krp3mpk3* indicates that *KRP3* and *MPK3* are involved in a single pathway and also confirms that *MPK3* functions upstream of *KRP3*, regulating rice morphogenesis and yield. These observations further strengthened the role of MAPK-mediated phosphorylation of KRP3 in cell cycle regulation.

Phenotyping of constitutively overexpressing transgenic lines of *KRP3* phospho-dead (*KRP3$^{AA}$-OE*) and phospho-mimetic (*KRP3$^{EE}$-OE*) form provided insights into the role of its phosphorylation in plant architecture and yield regulation. For the phospho-mimetic form of KRP3, Ser was converted to Glu (*KRP3$^{EE}$*), which mimics the negative charge imposed due to phosphorylation (Dóczi and Bögre 2018). A clear difference between *KRP3$^{EE}$* and *KRP3$^{AA}$* overexpression lines was observed, where *KRP3$^{EE}$-OE* lines exhibited a stronger reduction in plant height, internode length, and leaf length. This phenotype indicates that phosphorylation of KRP3 increases its potential to inhibit the cell cycle. Altogether, it can be concluded that KRP3 plays a crucial role in maintaining rice vigour and yield. The phosphorylation of KRP3 is critical to regulating the KRP3 protein turnover rate. It is also evident that maintaining KRP3 protein homeostasis in dividing cells is the decisive factor for cell division rate.

MAP Kinase signalling had diverse effects on its substrates due to phosphorylation, which includes modulating localization, gain or loss of function, or even affecting stability (Bhagat, Verma, et al. 2022; Kim et al. 2022). Some KRP proteins contain an NLS signal and get localised into the nucleus (Boruc et al. 2010). Rice KRP3 was also found to be localised in the nucleus. However, similar to KRP3, its phospho-dead, and phospho-mimetic versions were also found to be localised into the nucleus, indicating phosphorylation doesn't regulate the localization of KRP3. Further, phosphorylation doesn't seem to regulate the interaction of KRP3 with its target proteins. It is known that KRP3 interacts with the CDKA-CycD complex and inhibits its function (Mizutani et al. 2010). No change in the interaction between KRP3, KRP3$^{AA}$ and KRP3$^{EE}$ forms with CDKA and CycD was observed. Another aspect that regulates the function of KRPs is the protein turnover rate. Multiple mechanisms involving proteasomal and non-proteasomal mediated degradation govern the protein-level maintenance of KRPs (Kim et al. 2008; Li et al. 2016; Noir et al. 2015). MAP kinase-mediated phosphorylation also has implications for regulating protein turnover (Kim et al. 2022). In the case of KRP3, the cell-free degradation assay clearly showed that the stability of KRP3$^{EE}$ is significantly enhanced over KRP3 and KRP3$^{AA}$. Further in vivo degradation assay in the presence and absence of MG132, a potential inhibitor of proteasome, clearly indicated that KRP3 is a target of proteasome-mediated degradation. It was also evident that phosphorylation of KRP3 at positions 17 and 82 inhibits its degradation, as it inhibits its polyubiquitination.

Adequate protein level maintenance of some KRPs, in a dividing cell, is crucial in *Arabidopsis*. The level of AtKRP4 protein inherited from the parent regulates the onset and duration of subsequent cell divisions (D'Ario et al. 2021). Other than *AtKRP4*, overexpression of *AtKRP6* has been shown to promote cell division in roots infected by root-knot nematodes (Vieira et al. 2014). With this information, we re-examined our findings to validate that KRP3 regulates rice cell division in a dose-dependent manner. From the plant vegetative growth and yield parameters, it is evident that the *krp3* mutant and *KRP3-OE* or *KRP3$^{EE}$-OE* are showing similar phenotypes in several traits like plant height, root length, seed number, cell length, cell division rate, etc. Figure 7D represents a simplified model depicting the effect of KRP3 phosphorylation by MPK3 and its impact on rice plants. In conditions where KRP3 protein cannot get phosphorylated, i.e., *mpk3* or *KRP3$^{AA}$-OE*, a similar deviation from the normal phenotype was observed, but the reduction in plant growth and yield was less severe. This demonstrates that KRP3 functions in a dose-dependent manner to maintain cell division rate and cell size in rice-growing organs and requires MPK3-mediated phosphorylation for its stability. Phosphorylated KRP3 modulates cell proliferation in rice to maintain its plant architecture and yield-contributing traits.

## 4 | Materials and Methods

### 4.1 | Development of Phylogenetic Tree

Sequences of 144 monocot-specific KRP proteins were retrieved from the NCBI database. The phylogenetic tree was constructed using the Maximum Likelihood method and the JTT matrix-based model, with 100 bootstrap replicates. The MEGA11 platform was used for developing the tree (Tamura et al. 2021).

### 4.2 | Generation of Knockout, Overexpression and Promoter-Reporter Lines

Knockout mutants of *krp3, mpk3*, and *krp3mpk3* were developed as described by Singh, Sharma, et al. (2024); Singh, Verma, et al. (2024) and Xie et al. (2015) using the pRGEB32 vector. Transgenics were raised as previously described by Rengasamy et al. (2024) in Japonica rice (*Oryza sativa* Lin.) variety Taipei309 (TP309) background. Homozygous mutations were detected by DNA sequencing using the Sanger method. For the development of over-expression lines, KRP3, $KRP3^{AA}$, and $KRP3^{EE}$ fused with N-terminal 3xFLAG and C-terminal 4xMyc tag were cloned under the CaMV-35S promoter and NOS terminator into the pCAMBIA1300 vector. The developed construct and empty pCAMBIA1300 vector were transformed in EHA103, followed by stable transgenic development. For developing promoter-reporter lines, a 2 kb region upstream of the KRP3 coding sequence was cloned into pCAMBIA1301 using EcoRI and NcoI restriction sites, replacing the CaMV-35S promoter. The construct was transformed into TP309 to develop *ProKRP3::GUS lines*. pCAMBIA1301 devoid of the CaMV-35S promoter was used for *VC-GUS* line development. Primers used for the development of constructs are mentioned in Table S1.

### 4.3 | Measurement of Plant Morphological Parameters

Plants were grown in greenhouse conditions with a 16 h light and 8 h dark photoperiod cycle at 28°C ± 2°C temperature with 60% relative humidity till maturity. After maturity, five plants from each line were photographed to measure final plant height. Height was measured from the root initiation zone to the panicle end using ImageJ software. The primary tiller numbers of five mature plants were counted manually. Internodes were exposed by removing all leaves from the primary tiller, and then photographs were taken of all tillers from five mature plants. The 1st internode (identified as mentioned in Ji et al. (2019)) length of 20 internodes was measured using ImageJ software. Similarly, the fully grown last vegetative leaf (leaf immerged prior to the flag leaf) length was measured (from leaf tip to ligule) using ImageJ software.

### 4.4 | Measurement of Seed Parameters

Seed numbers of individual panicles of five plants were measured to determine the average seed number per panicle. For seed weight, a hundred seed weights were weighed using a Sartorius TE64 weighing balance. Seed length and width were measured using ImageJ by taking photographs of 10 seeds arranged in a line.

### 4.5 | Estimation of Cell Length and Width

Around 1 cm long root portion from the mature zone (below crown region) of 7-day-old seedlings was cut and incubated with 1 μg/mL Propidium Iodide (PI) visualised under a confocal microscope (SP8, Leica) for PI fluorescence. Cell wall autofluorescence was also captured as described by Lahlali et al. (2016) to determine cell boundaries. Cell length and width were measured using Leica LAS AF Lite software.

### 4.6 | GUS Staining

Seven-day-old seedlings and 1st internode region of ProKRP3::GUS and VC-GUS lines were incubated in GUS staining solution (200 μM of X-Gluc, 0.2 mM $K_3Fe(CN)_6$, 0.2 mM $K_4Fe(CN)_6$, 100 mM EDTA, 0.1% TritonX100, pH 7.0) for 12 h followed by destaining. Photographs were taken using a stereo zoom microscope equipped with a camera (Zeiss).

### 4.7 | EdU Labelling of Root and Shoot Tips

EdU was added to liquid growth media with a final concentration of 50 μM for incorporation into the growing root or shoot tip. Root or shoot tips were harvested after EdU and labelled with Alexa Fluor 594 dye using Click-iT EdU Cell Proliferation Kit (Invitrogen) as per the manufacturer's protocol. EdU incorporation was detected under a confocal microscope (SP8, Leica) with an excitation wavelength around 590 nm and an emission wavelength around 618 nm.

### 4.8 | Flowcytrometry and Genomic Content Analysis

Nuclei were isolated from a 1 mm portion of a 7-day-old seedling root tip by chopping in 1 mL ice-cold Galbraith's buffer (45 mM MgCl2, 20 mM MOPS pH 7.0, 30 mM sodium citrate, 0.1% [v/v] Triton X-100) supplemented with RNAse A (7 U/mL). Isolated nuclei were stained with propidium iodide at a final concentration of 100 μg/mL. The sample was analysed using the BD FACSLyric Flow Cytometry System, conditioned as described by Pedroza-Garcia et al. (2021). The percentage of 2C and 4C in each sample was calculated with the BD FACSuite Application.

### 4.9 | Cell Cycle Inhibitor Treatment and Expression Analysis of KRP3

For cell cycle inhibitor treatment to TP309 root, 4 mg/mL HU, 0.1 mg/mL mimosine, 15 μg/mL oryzalin, and 15 μg/mL propyzamide were added to the liquid growth media. After 4 h, root samples were harvested for KRP3 expression analysis as described previously by Jonwal et al. (2023). Two internal control genes, Ubq5 and Ef1a, were used.

### 4.10 | HU Sensitivity Assay in Rice Root

For HU sensitivity assay in rice roots, all lines were simultaneously grown with or without 2.5 mM HU in solid 1/2MS media. After 7 days, root length was measured. Percent reduction in root length was calculated with the following formula.

$$\text{Percent root length reduction} = ((\text{Root length in control } (-\text{HU}) - \text{root length in } +\text{HU})/\text{Root length in control}) \times 100$$

### 4.11 | Yeast Two-Hybrid Assay (Y2H)

Full-length KRP3 coding regions were cloned into pGBKT7 vectors. While MAP Kinases (MPK3, MPK4, and MPK6) cloned into pGADT7 have been reported previously by Singh, Sharma, et al. (2024); Singh, Verma, et al. (2024). The Y2H assay was conducted as described by Banerjee et al. (2023) previously. The fully grown colonies on quadruple dropout medium were noted as positive interactions.

### 4.12 | In Vitro Pull-Down Assay

For pull-down assay, KRP3 was cloned into the pGEX-4T-2 vector and transformed into the BL21-DE3-Rosetta strain for protein induction. GST-KRP3 protein, induced at 22°C for 12 h with 1 mM IPTG, was immobilised into glutathione Resin (G-Bioscience), as described by Banerjee et al. (2023). Immobilised KRP3 protein was used as prey while bacterially expressed, purified 6xHis-MPK3, 6xHis-MPK4, and 6xHis-MPK6 were used as bait. The pull-down assay and detection of protein using western blot were conducted as previously mentioned by Banerjee et al. (2023).

### 4.13 | Split Luciferase Complementation (SLC) Assay

SLC assay was conducted as described by Chen et al. (2008). For visualisation of interaction, constructs were agro-infiltrated (EHA105) into *N. benthamiana* leaf. Post 48 h, luciferase activity was detected by CCD camera (ChemiDoc Imaging Systems, Bio-Rad), using a luciferase assay system (Promega).

### 4.14 | Intracellular Protein Localization

For identification of KRP3 and its phosphor-dead and phosphor-mimetic forms localization, all three forms of KRP3 were cloned in frame with mCherry at its N-terminal site and 2A-NLS-mGFP at its C-terminal site. The construct was transiently transformed into *N. benthamiana* leaf. mCherry and GFP fluorescence were visualised 48 h post-infiltration under a confocal microscope.

### 4.15 | Bimolecular Fluorescence Complementation (BiFC) Assay

BiFC assay was carried out as described by Waadt et al. (2008) and Verma et al. (2021). In brief, constructs were agro-infiltrated (EHA105) into *N. benthamiana* leaves in their respective combinations along with helper construct P19. The leaves were observed 48 h post-infiltration using a confocal scanning microscope (TCS SP5, Leica) with YFP filters.

### 4.16 | Co-Immuno Precipitation Assay

Co-IP was performed as described by Verma et al. (2024), with some modifications. KRP3 (with N-terminal 3xFLAG and C-terminal 4xMYC tag) was used to co-precipitate GFP, GFP-MPK3, and GFP-MPK6. The construct expressing KRP3, in combination with GFP, GFP-MPK3, or GFP-MPK6, was transiently transformed into *N. benthamiana* leaves. Crude protein was isolated from the infiltrated leaves using protein isolation buffer containing 50 mM HEPES pH 7.5, 150 mM NaCl, 10 mM EDTA, 5% glycerol, 5 mM DTT, and 1× plant protease inhibitor cocktail (Sigma). Anti-FLAG antibody bound to Protein A—Sepharos 4B resin was used to precipitate KRP3. Precipitation of KRP3 was detected using anti-cMYC antibody (Invitrogen), while co-precipitants were detected using anti-GFP antibody (Abcam). HRP-anti-rabbit antibody (Invitrogen) was used for the detection of the primary antibody.

### 4.17 | In Vitro Kinase Assay

KRP3, MPK3, and AtMKK4 were cloned into the pGEX-4T-2 vector for GST-tagged protein expression. In vitro kinase assay was done as described by Jalmi and Sinha (2016). Proteins (kinase and substrate) were incubated with kinase reaction buffer (50 mM Tris–HCl, pH 7.5, 1 mM DTT, 10 mM $MgCl_2$, 10 mM $MnCl_2$, 50 mM ATP, and 0.037 MBq of ($\gamma^{32}$P ATP) [60 Ci/mmol]) at 30°C for 30 min. Kinase reactions were stopped after 30 min by adding 5X SDS loading dye and heated for 5 min at 95°C. Reaction products were run on SDS-PAGE gel and were analysed by autoradiography.

### 4.18 | In-Vivo Protein Phosphorylation Detection

Crude protein was isolated (as mentioned previously) from respective plant samples and separated in an 8%-SDS polyacrylamide gel supplemented with 40 μM of Phos-tag. KRP3 protein was detected using Anti-FLAG antibody (Sigma) and HRP-Anti-Mouse antibody (Invitrogen). Active MAPK level was detected using anti-pTEpY antibody (CST) and HRP-anti-rabbit (Invitrogen) antibody. HRP activity was detected using ECL substrate and the signal was captured using the iBright Imaging System (Invitrogen).

### 4.19 | Cell-Free Degradation Assay

Total plant protein (500 μg) isolated from TP309 seedling (in 50 mM HEPES pH 7.5, 150 mM NaCl, 10 mM EDTA, 5% glycerol, 5 mM DTT supplemented with 10 mM ATP) was incubated with 10 μg of KRP3, $KRP3^{AA}$, and $KRP3^{EE}$ (c-terminal 6xHis and n-terminal Maltose binding protein (MBP) tag) recombinant protein for different time points. KRP3 protein level was detected by western blotting with anti-6xHis antibody (Thermo Fisher).

### 4.20 | In Vivo Protein Degradation Assay

Isolated protoplasts of *KRP3-OE1*, *KRP3AA-OE1*, and *KRP3EE-OE1* were treated with 200 μM CHX along with or without 100 μM MG132 at different time points. Post-incubation, crude protein was isolated using protein isolation buffer (previously mentioned), and the protein was separated using a 10%-SDS polyacrylamide gel. KRP3 protein level was

detected using Anti-FLAG antibody (Sigma) and Anti-Mouse secondary antibody (Invitrogen). Actin level was detected using IB with Anti-Actin antibody (Sigma) and Anti-Mouse antibody (Invitrogen).

## 4.21 | In Vitro Ubiquitination Assay

Bacterially expressed GST and GST- KRP3, KRP3$^{AA}$ and KRP3$^{EE}$ were immobilised in glutathione sepharose 4B resin. Immobilised protein was incubated with plant (TP309) crude protein extract (containing 50 mM HEPES pH 7.5, 150 mM NaCl, 10 mM EDTA, 5% glycerol, 5 mM DTT, 10 mM ATP, 100 μM MG132, 1× protease inhibitor, and 0.1% (V/V) Triton X100). After 30 min incubation, resin was washed 5 times in protein isolation buffer. After washing, the resin was incubated with 2xSDS loading dye, and soluble protein was separated in a 10%-SDS polyacrylamide gel. Ubiquitination was detected by IB with anti-Ubiquitin antibody (Abcam). The input sample was detected using an anti-GST antibody.

## 4.22 | Statistical Analysis

One-way ANOVA with Tukey's multiple comparisons test or Dunn's multiple comparisons test has been conducted to determine the significance. A significant difference has been represented by the Compact Letter Display (CLD) method. Test results are mentioned in Table S2.

## 4.23 | Accession Numbers

KRP3: LOC_Os11g40030, MPK3: LOC_Os03g17700, CDKA1: LOC_Os03g02680, CycD2: LOC_Os07g42860.

### Author Contributions

G.B. and A.K.S. planned the study and designed the experiments. G.B. carried out most of the experiments. S.J. and B.R. helped in generating transgenic lines, and S.J., B.R., U.P., M.M., and D.S. helped in recording part of the phenotypic data. G.B. and A.K.S. analysed the data and wrote the manuscript. A.K.S. approved the final draft.

### Acknowledgements

G.B., U.P. and D.S. acknowledge the Council of Scientific and Industrial Research, Government of India, and BRIC-NIPGR for fellowship. S.J. acknowledges the Department of Biotechnology, Government of India for fellowship. A.K.S. thanks Sir JC Bose Fellowship from the Anusandhan National Research Foundation, Department of Science and Technology, Government of India (File no.: JCB/2020/000041). The work is partially supported by the grant from the Department of Biotechnology, Government of India (Grant No.: BT/PR26207/GET/119/120/2017). The authors also acknowledge the Gene Functional Analysis Platform for Crops, Confocal Facility, DNA sequencing facility, Radioisotope facility and the Central Instrumentation Facility of NIPGR, New Delhi, India.

### Conflicts of Interest

The authors declare no conflicts of interest.

### Data Availability Statement

The authors have nothing to report.

### References

Ajadi, A. A., X. Tong, H. Wang, et al. 2020. "Cyclin-Dependent Kinase Inhibitors KRP1 and KRP2 Are Involved in Grain Filling and Seed Germination in Rice (*Oryza sativa* L.)." *International Journal of Molecular Sciences* 21: 1–16.

Arendsee, Z. W., L. Li, and E. S. Wurtele. 2014. "Coming of Age: Orphan Genes in Plants." *Trends in Plant Science* 19: 698–708.

Banerjee, G., D. Singh, C. Pandey, et al. 2023. "Rice Mitogen-Activated Protein Kinase Regulates Serotonin Accumulation and Interacts With Cell Cycle Regulators Under Prolonged UV-B Exposure." *Plant Physiology and Biochemistry* 203: 108078.

Barrôco, R. M., A. Peres, A. M. Droual, et al. 2006. "The Cyclin-Dependent Kinase Inhibitor Orysa; KRP1 Plays an Important Role in Seed Development of Rice." *Plant Physiology* 142: 1053–1064.

Bhagat, P. K., D. Sharma, D. Verma, K. Singh, and A. K. Sinha. 2022. "Arabidopsis MPK3 and MPK6 Regulates D-Glucose Signaling and Interacts With G-Protein, RGS1." *Plant Science* 325: 111484.

Bhagat, P. K., D. Verma, K. Singh, R. Badmi, D. Sharma, and A. K. Sinha. 2022. "Dynamic Phosphorylation of miRNA Biogenesis Factor HYL1 by MPK3 Involving Nuclear–Cytoplasmic Shuttling and Protein Stability in Arabidopsis." *International Journal of Molecular Sciences* 23: 3787.

Boruc, J., E. Mylle, M. Duda, et al. 2010. "Systematic Localization of the Arabidopsis Core Cell Cycle Proteins Reveals Novel Cell Division Complexes." *Plant Physiology* 152: 553–565.

Burgess, A. J., C. Masclaux-Daubresse, G. Strittmatter, et al. 2023. "Improving Crop Yield Potential: Underlying Biological Processes and Future Prospects." *Food and Energy Security* 12: 1–29.

Chehrehasa, F., A. C. B. Meedeniya, P. Dwyer, G. Abrahamsen, and A. Mackay-Sim. 2009. "EdU, a New Thymidine Analogue for Labelling Proliferating Cells in the Nervous System." *Journal of Neuroscience Methods* 177: 122–130.

Chen, H., Y. Zou, Y. Shang, et al. 2008. "Firefly Luciferase Complementation Imaging Assay for Protein-Protein Interactions in Plants." *Plant Physiology* 146: 368–376.

Chen, P., N. De Winne, G. De Jaeger, M. Ito, M. Heese, and A. Schnittger. 2023. "KNO1-Mediated Autophagic Degradation of the Bloom Syndrome Complex Component RMI1 Promotes Homologous Recombination." *EMBO Journal* 42: e111980.

D'Ario, M., R. Tavares, K. Schiessl, et al. 2021. "Cell Size Controlled in Plants Using DNA Content as an Internal Scale." *Science* 372: 1176–1181.

De Schutter, K., J. Joubès, T. Cools, et al. 2007. "Arabidopsis WEE1 Kinase Controls Cell Cycle Arrest in Response to Activation of the DNA Integrity Checkpoint." *Plant Cell* 19: 211–225.

Dóczi, R., and L. Bögre. 2018. "The Quest for MAP Kinase Substrates: Gaining Momentum." *Trends in Plant Science* 23: 918–932.

Guo, T., K. Chen, N. Q. Dong, et al. 2018. "GRAIN SIZE AND NUMBER1 Negatively Regulates the OSMKKK10-OSMKK4-OSMPK6 Cascade to Coordinate the Trade-Off Between Grain NUMBER Per Panicle and Grain Size in Rice." *Plant Cell* 30: 871–888.

Jalmi, S. K., and A. K. Sinha. 2016. "Functional Involvement of a Mitogen Activated Protein Kinase Module, OsMKK3-OsMPK7-OsWRK30 in Mediating Resistance Against *Xanthomonas oryzae* in Rice." *Scientific Reports* 6: 1–14.

Ji, H., C. D. Han, G. S. Lee, et al. 2019. "Mutations in the microRNA172 Binding Site of SUPERNUMERARY BRACT (SNB) Suppress Internode Elongation in Rice." *Rice* 12: 62.

Jiang, M., X. Li, X. Dong, et al. 2022. "Research Advances and Prospects of Orphan Genes in Plants." *Frontiers in Plant Science* 13: 1–13.

Jonwal, S., B. Rengasamy, and A. K. Sinha. 2023. "Regulation of Photosynthesis by Mitogen-Activated Protein Kinase in Rice: Antagonistic Adjustment by OsMPK3 and OsMPK6." *Physiology and Molecular Biology of Plants* 29: 1247–1259.

Jonwal, S., N. Verma, and A. K. Sinha. 2022. "Regulation of Photosynthetic Light Reaction Proteins via Reversible Phosphorylation." *Plant Science* 321: 111312.

Kim, H. J., S. A. Oh, L. Brownfield, et al. 2008. "Control of Plant Germline Proliferation by SCFFBL17 Degradation of Cell Cycle Inhibitors." *Nature* 455: 1134–1137.

Kim, S. H., S. Bahk, N. T. Nguyen, et al. 2022. "Phosphorylation of the Auxin Signaling Transcriptional Repressor IAA15 by MPKs Is Required for the Suppression of Root Development Under Drought Stress in Arabidopsis." *Nucleic Acids Research* 50: 10544–10561.

Lahlali, R., S. Kumar, L. Wang, et al. 2016. "Cell Wall Biomolecular Composition Plays a Potential Role in the Host Type II Resistance to *Fusarium* Head Blight in Wheat." *Frontiers in Microbiology* 7: 1–12.

Li, G., J. Tang, J. Zheng, and C. Chu. 2021. "Exploration of Rice Yield Potential: Decoding Agronomic and Physiological Traits." *Crop Journal* 9: 577–589.

Li, L., B. Li, C. Xie, et al. 2020. "Arabidopsis RAD23B Regulates Pollen Development by Mediating Degradation of KRP1." *Journal of Experimental Botany* 71: 4010–4019.

Li, Q., X. Shi, S. Ye, et al. 2016. "A Short Motif in Arabidopsis CDK Inhibitor ICK1 Decreases the Protein Level, Probably Through a Ubiquitin-Independent Mechanism." *Plant Journal* 87: 617–628.

Liu, F., P. Wang, X. Zhang, et al. 2018. "The Genetic and Molecular Basis of Crop Height Based on a Rice Model." *Planta* 247: 1–26.

Lo, S. F., M. L. Cheng, Y. i. C. Hsing, et al. 2020. "Rice Big Grain 1 Promotes Cell Division to Enhance Organ Development, Stress Tolerance and Grain Yield." *Plant Biotechnology Journal* 18: 1969–1983.

Manna, M., B. Rengasamy, and A. K. Sinha. 2023. "Revisiting the Role of MAPK Signalling Pathway in Plants and Its Manipulation for Crop Improvement." *Plant, Cell & Environment* 46: 2277–2295.

Mizutani, M., T. Naganuma, K. Tsutsumi, and Y. Saitoh. 2010. "The Syncytium-Specific Expression of the Orysa; KRP3 CDK Inhibitor: Implication of Its Involvement in the Cell Cycle Control in the Rice (*Oryza sativa* L) Syncytial Endosperm." *Journal of Experimental Botany* 61: 791–798.

Nakamura, M., K. Naoi, T. Shoji, and T. Hashimoto. 2004. "Low Concentrations of Propyzamide and Oryzalin Alter Microtubule Dynamics in Arabidopsis Epidermal Cells." *Plant & Cell Physiology* 45: 1330–1334.

Noir, S., K. Marrocco, K. Masoud, et al. 2015. "The Control of *Arabidopsis thaliana* Growth by Cell Proliferation and Endoreplication Requires the F-Box Protein FBL17." *Plant Cell* 27: 1461–1476.

Pan, T., Q. Qin, C. Nong, et al. 2021. "A Novel WEE1 Pathway for Replication Stress Responses." *Nature Plants* 7: 209–218.

Pedroza-Garcia, J. A., T. Eekhout, I. Achon, et al. 2021. "Maize ATR Safeguards Genome Stability During Kernel Development to Prevent Early Endosperm Endocycle Onset and Cell Death." *Plant Cell* 33: 2662–2684.

Ren, H., A. Santner, J. C. Del Pozo, J. A. H. Murray, and M. Estelle. 2008. "Degradation of the Cyclin-Dependent Kinase Inhibitor KRP1 Is Regulated by Two Different Ubiquitin E3 Ligases." *Plant Journal* 53: 705–716.

Rengasamy, B., M. Manna, S. Jonwal, M. Sathiyabama, N. B. Thajuddin, and A. K. Sinha. 2024. "A Simplified and Improved Protocol of Rice Transformation to Cater Wide Range of Rice Cultivars." *Protoplasma* 261: 641–654.

Sethi, V., B. Raghuram, A. K. Sinha, and S. Chattopadhyay. 2014. "A Mitogen-Activated Protein Kinase Cascade Module, MKK3-MPK6 and MYC2, Is Involved in Blue Light-Mediated Seedling Development in Arabidopsis." *Plant Cell* 26: 3343–3357.

Singh, D., G. Banerjee, N. Verma, and A. K. Sinha. 2023. "MAP Kinases May Mediate Regulation of the Cell Cycle in Rice by E2F2 Phosphorylation." *FEBS Letters* 597: 2993–3009.

Singh, D., N. Verma, B. Rengasamy, G. Banerjee, and A. K. Sinha. 2024. "The Small RNA Biogenesis in Rice Is Regulated by MAP Kinase-Mediated OsCDKD Phosphorylation." *New Phytologist* 244: 1482–1497.

Singh, K., D. Sharma, P. K. Bhagat, S. Tayyeba, S. Noryang, and A. K. Sinha. 2024. "Phosphorylation of AGO1a by MAP Kinases Is Required for miRNA Mediated Resistance Against *Xanthomonas oryzae* Pv. Oryzae Infection in Rice." *Plant Science* 340: 111967.

Singh, P., and A. K. Sinha. 2016. "A Positive Feedback Loop Governed by SUB1A1 Interaction With MITOGEN-ACTIVATED PROTEIN KINASE3 Imparts Submergence Tolerance in Rice." *Plant Cell* 28: 1127–1143.

Song, S., G. Liu, F. Ma, and Z. Bao. 2022. "Brassinazole Represses Tomato Hypocotyl Elongation via Inhibition of Cell Division." *Plant Growth Regulation* 96: 463–472.

Spadafora, N., L. Perrotta, J. Nieuwland, et al. 2012. "Gene Dosage Effect of WEE1 on Growth and Morphogenesis From Arabidopsis Hypocotyl Explants." *Annals of Botany* 110: 1631–1639.

Takai, T. 2023. "Potential of Rice Tillering for Sustainable Food Production." *Journal of Experimental Botany* 75: 708–720.

Tamura, K., G. Stecher, and S. Kumar. 2021. "MEGA11: Molecular Evolutionary Genetics Analysis Version 11." *Molecular Biology and Evolution* 38: 3022–3027.

Tian, X., M. He, E. Mei, et al. 2021. "WRKY53 Integrates Classic Brassinosteroid Signaling and the Mitogen-Activated Protein Kinase Pathway to Regulate Rice Architecture and Seed Size." *Plant Cell* 33: 2753–2775.

Verma, D., P. K. Bhagat, and A. K. Sinha. 2020. "MKK3-MPK6-MYC2 Module Positively Regulates ABA Biosynthesis and Signalling in Arabidopsis." *Journal of Plant Biochemistry and Biotechnology* 29: 785–795.

Verma, D., P. K. Bhagat, and A. K. Sinha. 2021. "A Dual-Specificity Phosphatase, MAP Kinase Phosphatase 1, Positively Regulates Blue Light-Mediated Seedling Development in Arabidopsis." *Planta* 253: 1–13.

Verma, N., D. Singh, L. Mittal, G. Banerjee, S. Noryang, and A. K. Sinha. 2024. "MPK4-Mediated Phosphorylation of PHYTOCHROME INTERACTING FACTOR4 Controls Thermosensing by Regulating Histone Variant H2A.Z Deposition." *Plant Cell* 36, no. 10: 4535–4556.

Vieira, P., A. De Clercq, H. Stals, et al. 2014. "The Cyclin-Dependent Kinase Inhibitor KRP6 Induces Mitosis and Impairs Cytokinesis in Giant Cells Induced by Plant-Parasitic Nematodes in Arabidopsis." *Plant Cell* 26, no. 6: 2633–2647.

Waadt, R., L. K. Schmidt, M. Lohse, K. Hashimoto, R. Bock, and J. Kudla. 2008. "Multicolor Bimolecular Fluorescence Complementation Reveals Simultaneous Formation of Alternative CBL/CIPK Complexes In Planta." *Plant Journal* 56: 505–516.

Xie, K., B. Minkenberg, and Y. Yang. 2015. "Boosting CRISPR/Cas9 Multiplex Editing Capability With the Endogenous tRNA-Processing System." *Proceedings of the National Academy of Sciences of the United States of America* 112: 3570–3575.

Xu, H., L. Bartley, M. Libault, V. Sundaresan, H. Fu, and S. Russell. 2023. "The Roles of a Novel CDKB/KRP/FB3 Cell Cycle Core Complex in Rice Gametes and Initiation of Embryogenesis." *Plant Reproduction* 36: 301–320.

Yang, R., Q. Tang, H. Wang, et al. 2011. "Analyses of Two Rice (*Oryza sativa*) Cyclin-Dependent Kinase Inhibitors and Effects of Transgenic Expression of OsiICK6 on Plant Growth and Development." *Annals of Botany* 107: 1087–1101.

## Supporting Information

Additional supporting information can be found online in the Supporting Information section. **Figure S1:** Expression analysis of *KRP3* and *KRP6*. **Figure S2:** Screening of *krp3* mutant as well as *KRP3* overexpressing transgenic plant. **Figure S3:** KRP3 expresses in actively dividing rice tissues and regulate interned cell size. **Figure S4:**. Seed and seedling morphology of TP309, *krp3-1*, *krp3-2*, VC, *KRP3-OE1*, *KRP3-OE2*, *KRP3-OE3* lines. **Figure S5:** KRP3 operates at S phase check point. **Figure S6:** Detection of KRP3 phosphorylation by MPK3 and identification of specific site of phosphorylation. **Figure S7:** *mpk3* and *krp3mpk3* knockout line screening and identification. **Figure S8:** Effect of *mpk3* mutation in rice plant and seed morphology. **Figure S9:** Selection of krp3mpk3 knockout line and comparision of seed morphology with TP309, *krp3-1* and *mpk3-1*. **Figure S10:** Effect of *krp3*, *mpk3* and *krp3mpk3* mutation on seedling growth. **Figure S11:** Development and evaluation of vegetative growth parameter upon overexpression of $KRP3^{AA}$ and $KRP3^{EE}$. **Figure S12:** Determination of cell division rate and expression profile of other KRPs in TP309, VC, *KRP3-OE1* *$KRP3^{AA}$-OE1 and $KRP3^{EE}$-OE1* lines. **Figure S13:** Effect of phosphorylation on localization and interaction of KRP3. **Figure S14:** Effect of phosphorylation on stability of KRP3. **Table S1:** List of primers. **Table S2:** Statistical data.